DOKUZ EYLÜL UNIVERSITY
GRADUATE SCHOOL OF NATURAL AND APPLIED SCIENCES

MECHANICAL BEHAVIORS OF POLYMER COMPOSITES WITH ADDITION OF NANOPARTICLE TO RESIN

by

Batuhan ABİŞ

September, 2024

İZMİR

MECHANICAL BEHAVIORS OF POLYMER COMPOSITES WITH ADDITION OF NANOPARTICLE TO RESIN

A Thesis Submitted to the
Graduate School of Natural and Applied Sciences of Dokuz Eylül University
In Partial Fulfillment of the Requirements for Master of Science in
Department of Mechanical Engineering, Mechanics Program

by

Batuhan ABİŞ

September, 2024

İZMİR

THESIS EXAMINATION RESULT FORM

We have read the thesis entitled **"MECHANICAL BEHAVIORS OF POLYMER COMPOSITES WITH ADDITION OF NANOPARTICLE TO RESIN"** completed by **BATUHAN ABİŞ** under supervision of **PROF.DR. RAMAZAN KARAKUZU** and we certify that in our opinion it is fully adequate, in scope and in quality, as a thesis for the degree of Master of Science.

Prof.Dr. Ramazan KARAKUZU

Supervisor

Prof.Dr. Yusuf ARMAN

Jury Member

Asst.Prof.Dr. Hamza TAŞ

Jury Member

Prof. Dr. Okan FISTIKOĞLU

Director

Graduate School of Natural and Applied Sciences

ACKNOWLEDGMENT

I would like to express my sincere gratitude to my supervisor, Prof. Dr. Ramazan Karakuzu, for his invaluable guidance, unwavering support, and insightful feedback throughout the process of conducting my master's thesis. His expertise, encouragement, and dedication have been instrumental in shaping this research and navigating through its challenges.

I extend my heartfelt appreciation to Dr. Mehmet Korkmaz and Dr. Halis Kandaş for their invaluable assistance in producing and testing the samples used in this study. Their expertise, patience, and willingness to share their knowledge have significantly contributed to the quality and reliability of the research findings.

I would also like to thank my co-workers for their patient and my family for their endless love, encouragement, and understanding throughout this journey. Their unwavering support has been a constant source of motivation and strength for me.

Batuhan ABİŞ

MECHANICAL BEHAVIORS OF POLYMER COMPOSITES WITH ADDITION OF NANOPARTICLE TO RESIN

ABSTRACT

Enhancing the mechanical behavior of polymer composites by incorporating nanoparticles is a pivotal area of research with far-reaching implications. Polymer composites find extensive applications in various industries due to their lightweight nature, corrosion resistance, and high strength-to-weight ratio. However, to meet the ever-evolving demands of modern engineering applications, there is a pressing need to further enhance their mechanical properties. By introducing nanoparticles into the polymer matrix, researchers aim to improve aspects such as tensile strength, flexural strength, impact resistance, and fatigue performance. The unique properties of nanoparticles, such as high surface area-to-volume ratio and enhanced mechanical properties, offer promising opportunities to overcome the limitations of conventional polymer composites. Consequently, investigating the effects of nanoparticle incorporation on the mechanical behavior of polymer composites holds significant promise for advancing materials science and engineering, paving the way for the development of high-performance materials tailored to specific applications.

In this study, an intraply hybrid woven fabric containing flax and E-glass yarns was produced. In order for few layer graphene and TiO_2 nanoparticles at various concentrations (0, 1, 2 and 3 wt%) to be well dispersed in the epoxy resin, the mixture was homogenized using mechanical and ultrasonic mixers, respectively. Then, hybrid composites were produced by hand lay-up and vacuum bagging methods. Following the fabrication of composite materials, samples are prepared for testing in both tensile and compression modes. Furthermore, the evaluation of shear properties and the assessment of quasi-static indentation test across various crosshead speeds are conducted. SEM and FTIR analyses were also performed to examine failure behavior and chemical characteristic of the composite.

Keywords: Hybrid Woven fabrics, nanoparticle, hand lay-up, vacuum bagging, mechanical behavior, SEM, FTIR

REÇİNEYE NANOPARTİKÜL KATILMIŞ POLİMER KOMPOZİTLERİN MEKANİK DAVRANIŞLARI

ÖZ

Nanopartiküllerin eklenmesiyle polimer kompozitlerin mekanik davranışının arttırılması, geniş kapsamlı etkileri olan çok önemli bir araştırma alanıdır. Polimer kompozitler hafif olmaları, korozyona dayanıklılıkları ve yüksek mukavemet/ağırlık oranlarından dolayı çeşitli endüstrilerde geniş uygulama alanları bulmaktadır. Ancak modern mühendislik uygulamalarının sürekli gelişen taleplerini karşılamak için mekanik özelliklerinin daha da geliştirilmesine ihtiyaç duyulmaktadır. Araştırmacılar, nanopartikülleri polimer matrisine dahil ederek, çekme mukavemeti, eğilme mukavemeti, darbe direnci ve yorulma performansı gibi hususları geliştirmeyi amaçlamaktadırlar. Yüksek yüzey alanı/hacim oranı ve geliştirilmiş mekanik özellikler gibi nanopartiküllerin benzersiz özellikleri, geleneksel polimer kompozitlerin sınırlamalarının üstesinden gelmek için umut verici fırsatlar sunmaktadır. Sonuç olarak, polimer kompozitlerin mekanik davranışı üzerine nanopartikül katılımının etkilerinin araştırılması, malzeme bilimi ve mühendisliğinin ilerlemesi için önemli umut vaat etmekte ve belirli uygulamalara özel yüksek performanslı malzemelerin geliştirilmesinin önünü açmaktadır.

Bu çalışmada, keten ve E-cam elyaf iplikleri ile hibrit bir dokuma kumaş üretilmiştir. Çeşitli konsantrasyonlardaki (ağırlıkça % 0, 1, 2 ve 3) az katmanlı grafen ve TiO_2 nanopartiküllerin epoksi reçine içinde iyi bir dağılım göstermesi için sırasıyla mekanik ve ultrasonik karıştırıcılar kullanılarak karışım homojenize edilmiştir. Kompozitler elle yatırma ve vakumlu torbalama yöntemleri kullanılarak üretilmiştir. Kompozit malzemelerin imalatının ardından numuneler hem çekme hem de basma modlarında test edilmek üzere hazırlanmıştır. Ayrıca, kayma özelliklerinin değerlendirilmesi ve çeşitli çekme çenesi hızlarında yarı statik testin değerlendirilmesi gerçekleştirilmiştir. Kompozitin hasar davranışını incelemek ve kimyasal karakteristiğini belirlemek için SEM ve FTIR analizleri de yapılmıştır.

Anahtar kelimeler: Hibrit dokuma kumaşlar, nanopartikül, elle yatırma yöntemi, vakum torbalama, mekanik davranışlar SEM, FTIR

CONTENTS

Page

THESIS EXAMINATION RESULT FORM ii
ACKNOWLEDGMENT iii
ABSTRACT iv
ÖZ v
CONTENTS vi
LIST OF FIGURES viii
LIST OF TABLES xi

CHAPTER ONE - INTRODUCTION 1

1.1 Composite Materials 1
1.2 Classification of Composite Materials 2
1.2.1 Classification According to the Matrix Structure 2
1.2.1.1 Polymer Matrix Composites 2
1.2.1.2 Metal Matrix Composites 3
1.2.1.3 Ceramic Matrix Composites 3
1.2.2 Classification According to the Reinforcement Element 3
1.2.2.1 Fiber-Reinforced Composites 3
1.2.2.2 Particle-Reinforced Composites 4
1.2.2.3 Laminate Composites 4
1.3 Manufacturing Methods of Composites 4
1.3.1 Open Molding 4
1.3.2 Close Molding 5

CHAPTER TWO - PREVIOUS STUDIES 6

CHAPTER THREE - MATERIAL AND METHODS 11

3.1 Materials 11
3.1.1 Description of Materials 11
3.1.2 Source of Materials 11
3.2 Methods 14
3.2.1 Production of Hybrid Woven Fabric Consisting of Flax Yarn and E-Glass Fiber 14
3.2.2 Production of Nano Particle Reinforced Epoxy 18
3.2.3 Production of Nano Particle Added Hybrid Woven Fabric Composite 19
3.2.4 Preparation of Test Samples 20
3.2.5 Tensile Test 22
3.2.6 Compression Test 24
3.2.7 Shear Test 25
3.2.8 Quasi-Static Indentation Test 26
3.2.9 SEM Analyses 28
3.2.10 FTIR Analyses 31

CHAPTER FOUR - EXPERIMENT RESULTS AND DISCUSSION 32

4.1 Mechanical Test Results 32
4.1.1 Tensile Test Results 32
4.1.2 Compression Test Results 34
4.1.3 Shear Test Results 36
4.1.4 Quasi-Static Indentation Test Results 38
4.2 SEM Analysis Results 44
4.3 FTIR Analysis Results 46

CHAPTER FIVE CONCLUSIONS 49

5.1 Conclusions 49
5.2 Recommendations 50

REFERENCES 52

LIST OF FIGURES

Page

Figure 3.1 a) E-Glass Fiber, b) Flax Yarn 12

Figure 3.2 a) F1564 Epoxy Resin, b) F-3487 Hardener 12

Figure 3.3 a) Few Layer Graphene (FLG), b) Titanium Dioxide (TiO_2) 14

Figure 3.4 Warping Machine 15

Figure 3.5 Heddle Frames and Warn Reed 16

Figure 3.6 CCI Tech Evergreen II Weaving Machine 16

Figure 3.7 Weaving Process 17

Figure 3.8 Produced Woven Fabrics 17

Figure 3.9 2x2 Weave Structure, Warp Direction-0˚, Weft Direction-90˚ 18

Figure 3.10 Nano Particle and Epoxy 18

Figure 3.11 Mixing Process 19

Figure 3.13 Test Sample Cutting Template 21

Figure 3.14 Wet Cutting Saw 21

Figure 3.15 Prepared Test Samples 22

Figure 3.16 Tensile Test Sample 22

Figure 3.17 Shimadzu AG-X Tensile Test Machine 23

Figure 3.18 Tensile Test with Strain Gage 23

Figure 3.19 Compression Test Device with Apparatus 24

Figure 3.20 Compression Test Sample 25

Figure 3.21 Shear Test Setup 25

Figure 3.22 Shear Test Sample with Strain Gage 26

Figure 3.23 Schematics Illustration of a Load-Displacement Curve for Toughened Matrix Composites 27

Figure 3.24 Quasi-Static Indentation Test with Apparatus 28

Figure 3.25 Quasi-Static Indentation Test Sample 28

Figure 3.26 Scanning Electron Microscope ZEISS EVO HD15 29

Figure 3.27 SEM Test Samples 30

Figure 3.28 a) Coating Device and b) Coated Samples 30

Figure 3.29 FTIR Device Thermo Scientific NICOLET iS10 31

Figure 3.30 FTIR Test Samples 31

Figure 4.1 Tensile Stress-Strain Graph of Composites, a) with TiO_2 b) with Few Layer Graphene 32

Figure 4.2 Tensile Strength Graph of Composites with a) TiO_2, b) Few Layer Graphene 33

Figure 4.3 Modulus of elasticity Graph of Composites with a) TiO_2, b) Few Layer Graphene 34

Figure 4.4 Poisson's Ratio of composites with, a) TiO_2 b) Few Layer Graphene 34

Figure 4.5 Compression Stress-Displacement Graph of Composites with, a) TiO_2 , b) Few Layer Graphene 35

Figure 4.6 Compressive Strength Graph of Composites with a) TiO_2, b) Few Layer Graphene 35

Figure 4.7 Shear Stress- Displacement Graph of Composites with a) TiO_2 , b) Few Layer Graphene 36

Figure 4.8 Shear Strength Graph of Composites with a) TiO_2 , b) Few Layer Graphene 37

Figure 4.9 Shear Modulus Graph of Composites with a) TiO_2 , b) Few Layer Graphene..... 37

Figure 4.10 Energy – Displacement Graphs of TiO_2 Added Composites at, a) 1.25 mm/min, b) 5 mm/min, c) 10 mm/ min..... 38

Figure 4.11 Force – Displacement Graphs of Graphene Added Composites at, a) 1.25 mm/min, b) 5 mm/min and c)10 mm/ min..... 39

Figure 4.12 Maximum Penetration Forces of TiO_2 Added Composites..... 40

Figure 4.13 Maximum Penetration Forces of Graphene Added Composites..... 41

Figure 4.14 Energy-Displacement Graphs for TiO_2 Added Composites at, a) 1.25 mm/min, b) 5 mm/min and c) 10 mm/ min..... 42

Figure 4.15 Energy-Displacement Graphs for Graphene Added Composites at, a) 1.25 mm/min, b) 5 mm/min and c) 10 mm/ min..... 43

Figure 4.16 Total Absorbed Energy Graph for TiO_2 Added Composites..... 43

Figure 4.17 Total Absorbed Energy Graph for Graphene Added Composites..... 44

Figure 4.18 SEM Pictures of Neat Composite..... 45

Figure 4.19 SEM Pictures of TiO_2 Added Composite..... 45

Figure 4.20 SEM Pictures of Graphene Added Composite..... 45

Figure 4.21 FTIR Spectrums of TiO_2 Added Composites..... 47

Figure 4.22 FTIR Spectrums of Graphene Added Composites..... 48

LIST OF TABLES

Page

Table 3.1 F-1564 Resin Properties 13

Table 3.1 F-1564 Resin Properties 13

Table 3.3 Few Layer Graphene Data Sheet 14

Table 3.4 TiO_2 Data Sheet 14

Table 4.1 Maximum Penetration Force of TiO_2 Added Composites 40

Table 4.2 Maximum Penetration Force of Graphene Added Composites 41

Table 4.3 Total Absorbed Energy Graph for TiO_2 Added Composites 43

Table 4.4 Total Absorbed Energy Graph for Graphene Added Composites 44

CHAPTER ONE
INTRODUCTION

1.1 Composite Materials

A composite material is one that do not macroscopically dissolve into another material after at least two distinct elements (a matrix and a reinforcing element) are combined. The substance that is mixed into the matrix is the reinforcing element. The material used for reinforcement can take the shape of flakes, particles, or threads. Typically, matrix material is continuous. Fibers in epoxy, steel rods in concrete, and other materials can be provided as examples of composites.

Nowadays, the necessity for composite materials with outstanding qualities has grown even more due to the shortcomings of traditional materials. Because of its advantages in terms of material strength, specific gravity, chemical and water resistance, simplicity of manufacture, and aesthetic appearance, composite materials are manufactured in response to these needs. For instance, composite material is widely utilized in aviation applications to achieve the high strength needed from vehicles without adding to the structure's weight. (Kaw, 2005)

Composite materials offer high specific stiffness and strength, significantly reducing component weight and providing a distinct advantage over traditional materials. They are energy-efficient, especially polymer-based composites, which are produced at relatively low temperatures. This efficiency, combined with their high specific hardness, makes composites ideal for use in airplanes and automobiles, enhancing fuel efficiency by reducing vehicle weight. Additionally, polymer matrix composites are more resistant to ambient conditions than metals, as only the polymer matrix contacts the air. Composites are also advantageous in applications requiring material properties in specific directions and in manufacturing parts with complex shapes, as they can be produced at or slightly above room temperature (around 150°C) and this makes composite more energy efficient. (Balasubramanian, 2014)

1.2 Classification of Composite Materials

In order to create composite materials, two different constituents are combined to provide superior qualities that neither component could provide alone. These two components are reinforcement element and matrix structure (Strong , 2006).

1.2.1 Classification According to the Matrix Structure

The choice of matrix material and the expected qualities of the composite are key constraints. The reinforcing elements are covered and supported by the matrix structure, which also distributes stresses among them and shields them from mechanical wear and environmental damage. The reinforcement is held together and the matrix provides the shape and form of the composite. Metals, ceramics, and polymers can all be used to create matrices.

1.2.1.1 Polymer Matrix Composites

The most widely utilized matrix in composite materials is made of polymers due to their low cost, ease of manufacturing, and adaptability. The thermoplastic resins and thermoset resins are the two main groups into which they can be separated.

Thermoplastics, as opposed to thermosets, can be heated and reformed repeatedly. They have been recognized for being recyclable, easy to process, and impact-resistant. Common varieties, which are utilized in anything from consumer goods to high-performance industrial parts, include polyethylene, polypropylene, and PEEK.

Polymers known as thermosets cannot be remelted or remolded because, once they cure, they generate irreversible chemical linkages. Superior mechanical qualities, outstanding chemical resistance, and exceptional thermal stability are the key characteristics of thermosets. They are used in industries like aerospace and automotives that demand high-strength, long-lasting materials (Mallick, 2007). Because of its special qualities, epoxy is perfect for a variety of uses, especially those requiring high performance, resistance, and durability and for these reasons, it was used in composite production in this research.

1.2.1.2 Metal Matrix Composites

In Metal Matrix Composites, a metal matrix is combined with a reinforcing substance, usually whiskers, fibers, or particles. The matrix is typically made of an alloy of titanium, magnesium, or aluminum, which has advantages in terms of strength, stiffness, and heat conductivity. Benefits include improved wear resistance and a high strength-to-weight ratio, making them perfect for sophisticated technical applications. Difficulties with joining MMCs with other materials, processing, and high production costs (particularly for continuous fiber reinforcements) are among the challenges.

1.2.1.3 Ceramic Matrix Composites

Ceramic Matrix Composites (CMCs) are materials having ceramic fibers embedded in a ceramic matrix that provide wear resistance, thermal shock resistance, and stability at high temperatures. CMCs are widely used in industries that require great performance under harsh conditions, including energy production (in nuclear reactors and solar plants), aerospace (for turbine blades), and automotive (for high-performance brakes and engine components).

1.2.2 Classification According to the Reinforcement Element

The composite gains strength and stiffness from the reinforcement element. It is the part that carries the load and greatly improves the matrix's mechanical qualities. The overall qualities of the composite are influenced by the kind, shape, and orientation of reinforcement used (Jones, 1999)

1.2.2.1 Fiber-Reinforced Composites

Continuous fiber composites have great strength and stiffness along the direction of the fibers because they use continuous and aligned fibers. Carbon fibers, glass fibers (like E-glass and S-glass), and aramid fibers (like Kevlar) are examples of common materials. Fibers with a random orientation or short length are seen in short fiber or whiskers composites. While they are simpler to produce and shape, they are typically not as strong as continuous fiber composites.

1.2.2.2 Particle-Reinforced Composites

Larger particles known as "macroscopic particle reinforcements" increase the modulus and compressive strength without appreciably affecting weight. Usually, they are utilized in situations where increased mechanical strength and wear resistance are necessary.

It is possible to dramatically change physical qualities including electrical conductivity, thermal stability, and wear resistance by adding microscopic or nanoparticle reinforcements. These tiny particles' interactions with the matrix have the potential to enhance performance in a range of applications, including sophisticated.

1.2.2.3 Laminate Composites

Multilayer laminate composites can have varying fiber kinds or orientations between their layers. Because of its layered structure, the composite can display customized qualities in particular directions, which makes it very helpful in structural applications where the ability to support weight is essential.

1.3 Manufacturing Methods of Composites

Depending on the kind of reinforcement and matrix utilized, the intended uses and attributes of the finished product, and other factors, different production techniques can be used for polymer composites. One helpful way to group the different techniques based on how the composite material is exposed throughout the production process is to divide the operations into open molding and closed molding (Krishan & Chawla, 2012)

1.3.1 Open Molding

Processes where the composite materials are exposed to air during manufacture are referred to as open molding. Though these techniques can be more labor-intensive and may not provide as much control over external elements like dust or humidity, which may negatively impact the quality, they are usually easier to use and less expensive than closed molding.

Hand Lay-up process is a manual process where fibers are placed in a mold and resin is applied by hand. It's flexible and cost-effective but labor-intensive and potentially inconsistent.

Spray-up process is similar to hand lay-up but utilizes a chopper gun to spray a mixture of resin and chopped fibers onto the mold. It offers faster production than hand lay-up but provides less control over fiber placement.

In Filament Winding process, fibers soaked in resin are wound around a rotating mandrel to create hollow, cylindrical shapes. This automated process is ideal for making items like tanks and pipes but is restricted to axisymmetric parts.

1.3.2 Close Molding

Resin Transfer Molding (RTM) process is a closed-mold process where fibers are placed in a mold, and resin is injected under pressure. It produces high-quality parts with excellent surface finish and good dimensional control but requires higher tooling costs.

Resin Transfer Molding (RTM) is a closed-mold process where fibers are placed in a mold, and resin is injected under pressure. Although it needs more expensive tooling, it provides high-quality products with good dimensional control and a perfect surface polish.

Using Compression Molding involves putting prepreg ingredients into a hot mold that ensures the part is formed by pressure. Although it requires a large initial investment, it is appropriate for high-volume manufacture of simple shapes and has good dimensional stability.

Vacuum Bagging process is part of the hand lay-up process, it becomes a closed method when a vacuum bag is used to compress the lay-up during curing.

The resin is forced into the dry fibers using vacuum pressure in a sealed mold during the vacuum infusion process, guaranteeing full saturation and few voids.

CHAPTER TWO
PREVIOUS STUDIES

The use of nanoparticles to improve polymer composites has attracted a lot of attention recently since there is an increasing need for materials with better mechanical properties in a range of engineering applications. Because of its excellent strength-to-weight ratio, corrosion resistance, and lightweight design, polymer composites are used extensively. Yet, in order to satisfy the exacting standards of contemporary technology, their mechanical behavior must be further improved, which has prompted researchers to look at new approaches. Adding nanoparticles to the polymer matrix is one method that shows promise for improving tensile strength, shear strength, and impact resistance.

This chapter examines relevant studies on the manufacturing and performance of hybrid polymer composites reinforced with synthetic and natural fibers, as well as the contribution of nanoparticles to the enhancement of these composites' characteristics. The following sections provide an overview of the main conclusions drawn from earlier research, emphasizing the approaches, materials, and results that have influenced our current understanding of nanoparticle-reinforced polymer composites. The experimental studies conducted in this thesis, which seek to further the continuing progress in materials science and engineering, are based on this review.

P. Prabhu et al. used Lannea coromandelica mixed with epoxy resin as the matrix material to study the dynamic mechanical properties of hybrid composites reinforced with natural fibers (silk, pineapple, flax) and synthetic fibers (glass). Using fiber mats that had been treated with NaOH or not treated, the composites were created using the compression hand molding process. Bentonite nano clay (BNC) was added in 2%, 4%, and 6% volume fractions. Important discoveries show that, in comparison to untreated samples, treated P/G/P fiber mats containing these BNC fractions have the best mechanical qualities, greatly increasing tensile strength, flexural strength, and impact strength. Results from dynamic mechanical analysis (DMA) showed that treated composites have the lowest damping factor (Tan δ) and maximum storage modulus, while biodegradability tests showed little weight loss over time, especially with 4% BNC. (Prabhu, Karthikeyan, Ravi Raja Malar Vannan, & Balaji, 2021)

Abd El-Baky et al. examined the mechanical characteristics of epoxy composites reinforced with flax, basalt, and E-glass fibers using the vacuum bagging technique. The goal of the study was to determine how these fibers' relative quantities and stacking order affected their tensile, flexural, and impact capabilities. The mechanical properties significantly improved when basalt and/or glass fiber reinforced epoxy laminas were used in place of partial flax fiber/epoxy laminas, according to the results. In comparison to composites with flax fibers in the outer layers, those with glass fibers in the outer layers showed the highest mechanical qualities, improving flexural and impact resistances but lowering tensile properties. The technique included reinforcing plain weave E-glass fabrics, 2x2 twill basalt, and woven flax fabrics with Kemapoxy 150 RGL epoxy resin. Eleven composite laminates were made and put through testing using various stacking configurations. To detect failure mechanisms, tensile, flexural, and impact tests were performed in addition to SEM examination. The study came to the conclusion that hybridizing glass and basalt fibers with flax fiber reinforced composites greatly improved their mechanical properties, and that the stacking order greatly affected the final product's overall performance. The results show promise for creating high-performing, cost-effective hybrid composites with customized mechanical characteristics for particular uses. (Abd El-Baky, Attia, Abdelhaleem, & Hassan, 2022)

Rapeephun Dangtungee and Suchart Siengchin examined the mechanical and thermal characteristics of hybrid composites made of silicon dioxide (SiO_2) generated by the hot-press process, polypropylene (PP) or high-density polyethylene (HDPE), and various flax fiber structures (unidirectional, biaxial, and twill). The surface of flax fibers was sprayed with SiO_2 particles, and the produced composites performed a number of tests, including as creep, stress relaxation, dynamic mechanical thermal analysis (DMTA), and thermogravimetric analysis (TGA). The study found that adding SiO_2 particles greatly improved the mechanical and thermal properties of flax fiber-reinforced PP and HDPE composites. The enhanced characteristics are ascribed to the polymer matrix's reduced chain mobility and improved interfacial bonding. The results show promise for creating high-performing, environmentally acceptable hybrid composites with specialized features for certain uses. (Siengchin & Dangtungee, 2014)

Meenakshi C.M. and Krishnamoorthy A. studied the fabrication and mechanical properties of hybrid composite laminates reinforced with glass and flax fibers in a polyester resin matrix. Hand lay-up is a basic and economical way of fabricating composites. The results showed that HFRP composites performed noticeably better than NFRP while having mechanical qualities similar to GFRP and somewhat lower tensile and flexural strengths. While HFRP's water absorption was considerably lower than NFRP's, it was somewhat greater than GFRP's, and its impact strength was almost identical to that of GFRP. This suggests that in applications where weight and environmental issues are crucial, HFRP composites may serve as an instantaneous replacement for GFRP. (Meenakshi & Krishnamoorthy, 2018)

Omkumar Meenakshisundaram and Srinivasan Shanmugam examined the impact of adding graphene to flax/E-glass/epoxy hybrid fiber-reinforced polymer (HFRP) composites. They used a compression molding process to manufacture the composites and change the weight percentage of graphene (0.0, 0.3, 0.6, 0.9, and 1.2 wt.%). Significant gains were seen in the investigation for the following parameters: impact strength (50%) tensile strength (86%), flexural strength (85%), shear strength (43%), shore D hardness (26%), and interlaminar shear strength (80%) at 0.6 weight percent graphene. Furthermore, the uniform dispersion of graphene led to a considerable decrease in water absorption and improved thermal stability, as thermogravimetric analysis (TGA) demonstrated. Fourier-transform infrared spectroscopy (FTIR) confirmed that the flax fibers' surface treatment increased bonding. According to the study's results, graphene-filled HFRP composites have better mechanical and thermal qualities, which qualifies them for use in high-performance industries like structural engineering and automotive. (Shanmugam & Meenakshisundaram, 2023)

Naheed Saba et. all examines the benefits of employing natural fibers and nano fillers in polymer hybrid composites to improve their mechanical qualities and environmental advantages. A major point raised by the review is that natural fibers are biodegradable, and because of their greater aspect ratio and wider surface area, nanocomposites have better qualities than natural fibers. Packaging, automotive, aerospace, and construction are just a few of the industries that the methodology's

applications in for are summarized, along with a variety of natural fibers and nanofillers. Hybrid bio-based composites, according to the authors, offer new business and technological prospects in a variety of industries and have a great deal of potential as sustainable materials. (Saba, ahir, & Jawaid , 2014)

An experimental investigation was carried out by Borra N. et all, to evaluate the impact of graphite loading on the mechanical characteristics of E-glass/flax epoxy hybrid polymer composites. They created laminates with different loadings of graphite particles using a hand layup vacuum bagging technique, and they tested the laminates' tensile and compressive strengths in accordance with ASTM guidelines. According to the investigation, the mechanical properties were enhanced by the addition of graphite. At 9% graphite loading, the greatest compressive strength of 477.61 MPa and tensile strength of 187.45 MPa were recorded. The results were also impacted by the stacking order, where the highest compressive strength was shown in the opposite arrangement and the best tensile strength was demonstrated by E-glass as the skin layer and treated flax as the core layer. Graphite greatly improves the characteristics of hybrid composites, making them appropriate for medium load structural applications, according to surface plots and Pareto charts. The authors' conclusion was that in order to improve the mechanical performance of polymer composites, hybridization with graphite is advised. (Dhanunjayarao, Naidu, Phaneendra, & Murty, 2022)

Anupama Hiremath et al. investigated the effects of incorporating TiO_2 nanoparticles into glass fiber/epoxy composites, focusing on interfacial interactions using dynamic mechanical analysis (DMA). The study revealed that adding TiO_2 nanoparticles significantly improved the storage modulus and loss modulus, enhancing the rigidity and thermal stability of the composites. The optimal TiO_2 loading was found to be 2 wt.%, which showed the highest storage modulus and cross-link density, indicating improved interfacial bonding and reduced molecular mobility. Higher TiO_2 loadings resulted in nanoparticle agglomeration, reducing the composite's mechanical performance. The study concluded that TiO_2 nanoparticles at 2 wt.% loading significantly enhance the mechanical properties and thermal stability of glass fiber/epoxy composites, making them suitable for applications requiring high-performance materials. (Hiremath, ve diğerleri, 2023)

Hiremath et all investigated the synergistic effects of ZnO and TiO_2 nanoparticles on the mechanical characteristics and thermal stability of glass fiber-reinforced LY556 epoxy composites. The hand layup method and vacuum curing were used to create the composites, which had different loadings of nanoparticles ranging from 1 to 5 wt.%. Up to 2 wt.% of nanoparticles were evenly dispersed, according to atomic force microscopy (AFM); larger loadings caused significant agglomeration. Mechanical testing revealed that impact strength was considerably increased by adding ZnO and TiO_2 nanoparticles, compared to tensile and flexural strengths. It was discovered that a 2 wt.% nanoparticle loading produced the best mechanical performance in terms of strength gains. When nanoparticles were incorporated, thermogravimetric analysis (TGA) revealed improved thermal stability, especially at higher loadings. According to the study's findings, adding 1 wt.% of ZnO and TiO_2 nanoparticles to the composites successfully improves their mechanical and thermal characteristics, qualifying them for high-performance uses. (Thipperudrappa, Hiremath, & Nagaraj, 2021)

CHAPTER THREE
MATERIAL AND METHODS

This chapter presents an in-depth description of the materials and methods utilized in the research. The objective is to facilitate the replication of the study by fellow researchers and to uphold the validity and reliability of the results.

The focus is on the integration of few layer graphene and TiO_2 nanoparticles into an epoxy resin matrix reinforced with a hybrid woven fabric of flax yarn and e-glass fiber and investigate material properties of this new material. The methods used in the experiments to evaluate the mechanical characteristics and examine the nanoparticle distribution in the composites are explained.

3.1 Materials

3.1.1 Description of Materials

The primary materials used in this research include:

- **Reinforcement Fabric**: A hybrid woven fabric consisting of Flax and E-glass yarns.
- **Matrix Material**: Epoxy resin.
- **Nanoparticles**: Few Layer Graphene (FLG) and Titanium Dioxide (TiO_2) nanoparticles.

3.1.2 Source of Materials

As reinforcement materials, the flax yarn was sourced from Nil-As Keten, Istanbul, Turkey and it has 210 Tex linear density and 100 % flax content. And the E-glass yarn, which has 300 Tex linear density, sourced from ŞİŞECAM (see Figure 3.1).

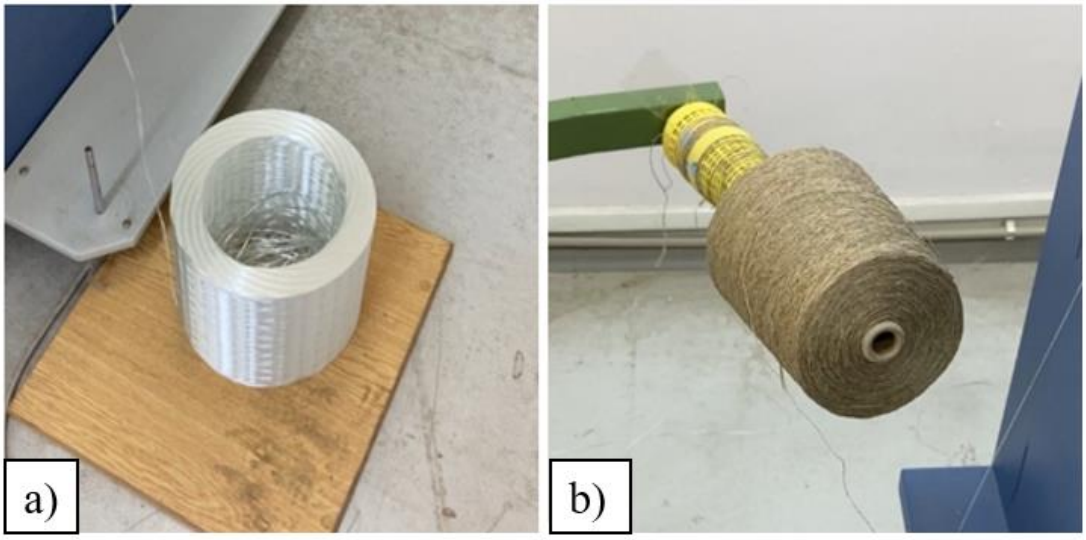


Figure 3.1 a) E-Glass Fiber, b) Flax Yarn

F1564 epoxy resin and F-3487 hardener were supplied obtained from FİBERMAK company were used as matrix materials (see Figure 3.2). Resin and Hardener properties is shown in the Table 3.1 and Table 3.2 respectively.



Figure 3.2 a) F1564 Epoxy Resin, b) F-3487 Hardener

Table 3.1 F-1564 Resin Properties

Appearance	Clear - Liquid				
Color	Transparent				
Viscosity (25 ˚C)	1200-1400		m.Pa.s		
Density (25 ˚C)	1.15		g/cm^3		
Curing	23 ˚C		2 Days		
	80 ˚C		4 Hours		
	100 ˚C		2 Hours		
Shelf Life (Room Temperature)	12		Month		
Package / Kg	1	5	10	20	25
Mixing Ratio (By Weight)	F-1564 Resin				100
	F-3486-3487 Hardener				34

Table 3.1 F-1564 Resin Properties

Appearance	Clear - Liquid				
Color	Transparent				
Viscosity (25 ˚C)	30-70		m.Pa.m		
Density (25 ˚C)	1		g/cm^3		
Curing	23 ˚C		2 Days		
	80 ˚C		4 Hours		
	100 ˚C		2 Hours		
Shelf Life (Room Temperature)	12		Month		
Package / Kg	1	5	10	20	25
Mixing Ratio (By Weight)	F-1564 Resin				100
	F-3486-3487 Hardener				34

The reinforcement particle materials used are few layer graphene (FLG), it's approximately 1 micrometer lateral size and titanium dioxide (TiO_2) nanoparticles, it's approximately 40 nanometers. They were supplied from graphenexpress company. The particles are shown in Figure 3. 3 and FLG and TiO_2 particles' properties shown in the Table 3.3 and Table 3.4 respectively.



Figure 3.3 a) Few Layer Graphene (FLG), b) Titanium Dioxide (TiO_2)

Table 3.3 Few Layer Graphene Data Sheet

Form	Powder
Color	Black
Dispersibility	Polar Solvent (DMF, NMP, etc.)
Conductivity (S/m)*	2250 ± 100
Spesific Surface Area (m2/g)	450±50
Elemental Composition (wt.%)	C: 97±0.5
	O: 3±0.5
*4-point-probe measurement on pellets (compressed under 5 tonnes for 10 minutes)	

Table 3.4 TiO_2 Data Sheet

Form	Powder
Color	White
Phase	Anatase
Dispersibility	Butanone, Daxad+DI
Purity	> 99%
BET (SSA)	75 g/cm3
Particle Size	40±5 nm

3.2 Methods

3.2.1 Production of Hybrid Woven Fabric Consisting of Flax Yarn and E-Glass Fiber

In the study, the intra-ply hybrid woven fabric was planned to produce with the E-glass and flax yarns, which were used as warp and weft yarns, respectively. The fabric manufacture starts with the warping process. Thanks to the warping machine, 420

warping yarns were prepared. The warping machine, shown in Figure 3.4, was used to transfer the E-glass yarns from the bobbin to the warp beams. Because of the diameter of warping machine, 180 cm warp yarns can be transferred from bobbin to the beam and the fabric can be obtained as 160 cm.

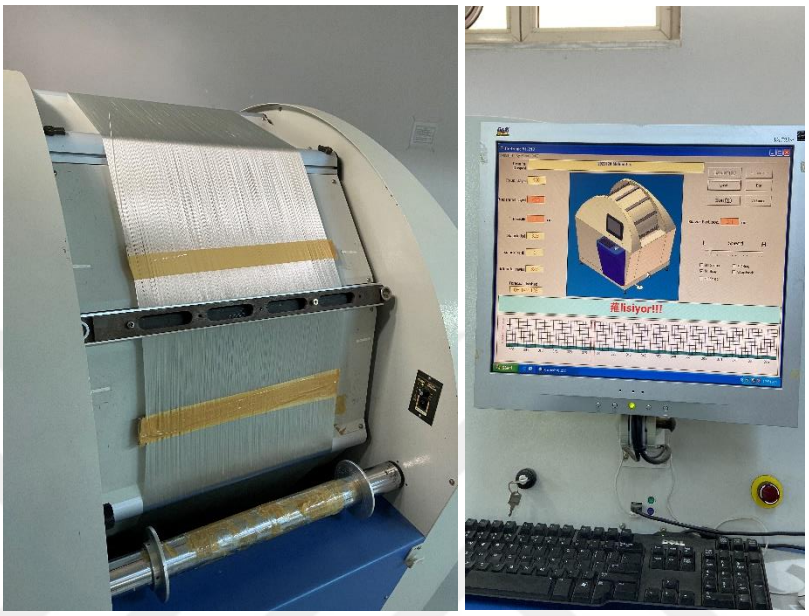


Figure 3.4 Warping Machine

Following the completion of the warping process, each yarn was passed from the heddle eyes through the drawing process. Deu to the 2x2 Twill weave pattern purposed to obtained, four heddle frames were utilized. Figure 3.5 displays the yarns, heddle frames, and drawing procedure. The gloves and mask were used throughout all procedures as the e-glass fibers are harmful for human health. A fabric with a width of 42 cm was produced.



Figure 3.5 Heddle Frames and Warn Reed

The automated CCI Tech Evergreen II weaving machine was used to create the fabrics from the e-glass and flax yarns. In Figure 3.6, the weaving machine is displayed.



Figure 3.6 CCI Tech Evergreen II Weaving Machine

After the weaving preparation processes were completed, the warp bobbin, the heddle frames and warp reed were connected to the machine for fabric production. All mechanisms in the machine can be actuated by manually or automatically from the computer. In every step of woven fabric production, the frames are opened according to the weave pattern. In this stage, the weft yarn is added. Thanks to the movement of reed, the added weft yarn is included to woven structure and the fabric is produced. The process is shown in Figure 3.7.



Figure 3.7 Weaving Process

In order to produce a fabric that reinforced the composites, the 2x2-twill weave pattern was selected. The warp and weft densities of fabric were settled as 10 yarns per cm. The fabrics that are shown in Figure 3.8 were obtained with dimensions of 1600 mm x 420 mm.



Figure 3.8 Produced Woven Fabrics

The produced fabric woven in a 2x2 weave is shown in Figure 3.9.

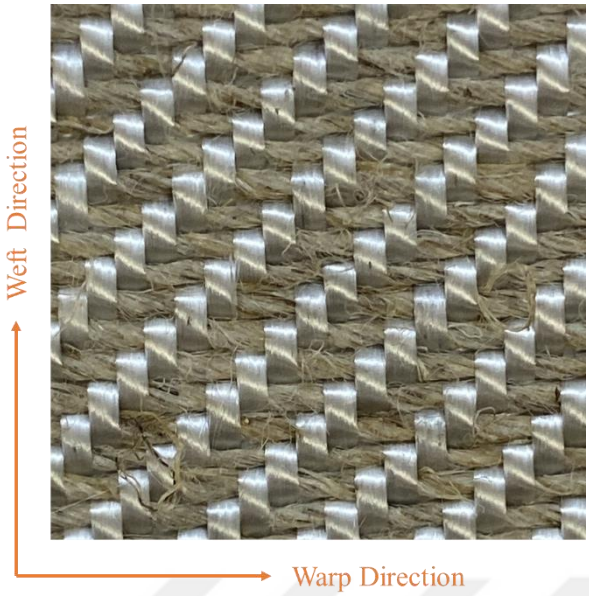


Figure 3.9 2x2 Weave Structure, Warp Direction-0˚, Weft Direction-90˚

3.2.2 Production of Nano Particle Reinforced Epoxy

The weight of the matrix material was initially determined during manufacture based on the fiber content. Subsequently, the epoxy resin was mixed with the appropriate amount of particles based on the determined matrix weight. It is shown in Figure 3.10.



Figure 3.10 Nano Particle and Epoxy

Afterwards, the matrix/particle composition was prepared using mechanical and ultrasonic mixing processes. Epoxy resin and particles were combined in the first stage of mixing using a mechanical mixer running at 250 rpm for five minutes. The Everest

CleanEx2511 ultrasonic bath device (400 kHz) at the Department of Metallurgical and Materials Engineering, Dokuz Eylül University, was utilized for the secondary mixing procedure. The epoxy resin and particle mixture were combined in this mixer for half an hour. It is shown in the Figure 3.11. Finally, hardener was added to this mixture and mixing was continued for another 10 minutes. This process was done for both graphene and TiO_2 nano-additives for 1-2-3 wt.% percent nano-additive material.



Figure 3.11 Mixing Process

3.2.3 Production of Nano Particle Added Hybrid Woven Fabric Composite

The fibers and matrix/particle mixture are manually mixed in the hand lay-up method used to produce composite materials. 600 mm x 600 mm teflon layer was laid at the bottom due to its fireproof properties. The paste was drawn as a frame. To guarantee uniform particle distribution, the produced matrix/particle mixture was first applied equally to each fiber layer. It consists of 4 layers of composite fabric, and the fabric directions are accordingly [0˚/90˚/90˚/0˚] The peeling ply was laid. Spiral hoses were placed through which the matrix mixture would be spread. Vacuum bag laid. Vacuum pipes through which the matrix mixture will flow T-shaped connection. Afterwards, the prepared fiber, matrix and particle arrangement was vacuumed. The vacuumed composite material was formed into a composite plate with a curing process lasting 8 hours at 80°C. The production stages of composites produced by hand lay-up and vacuum bagging processes are given in Figure 3.12.

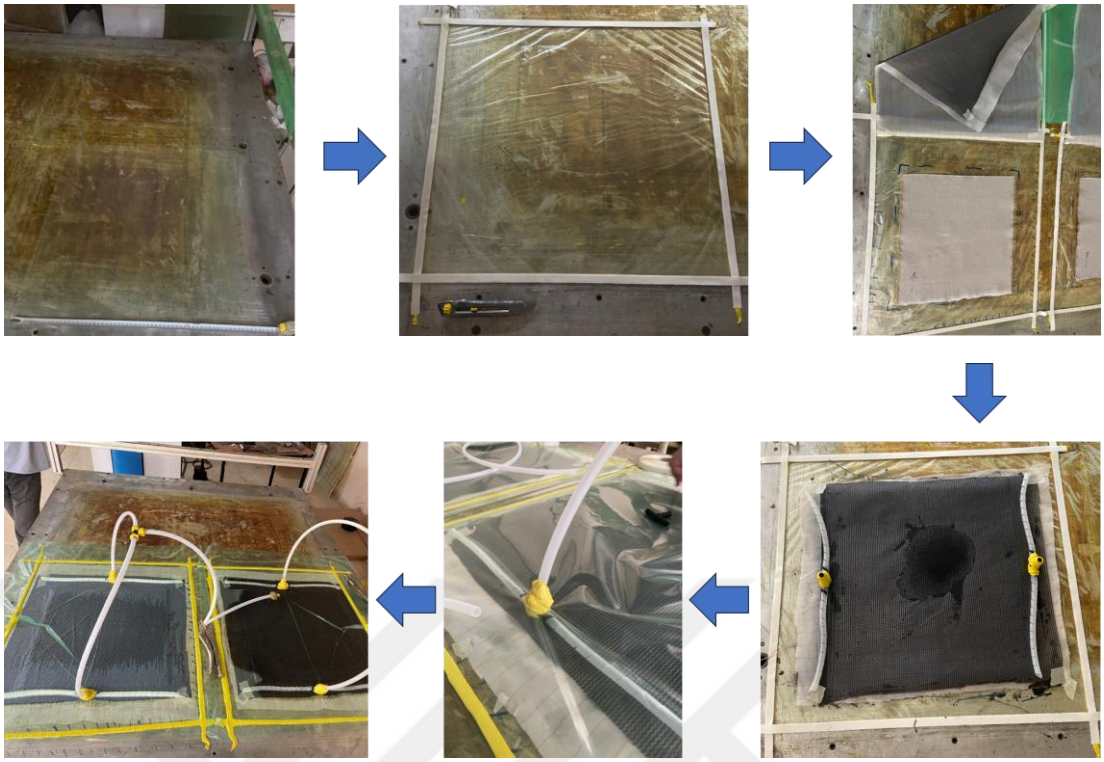


Figure 3.12 Composite Production Process

3.2.4 Preparation of Test Samples

The testing ASTM standards were followed in the preparation of the testing samples. The test sample template was created using the Solidworks program to fit inside the produced composite plate and into a 400mm x 400mm frame. The composite plates produced are 3.1 mm thick. In general, all tests were repeated 3 times. The drawn template is shown in Figure 3.13.

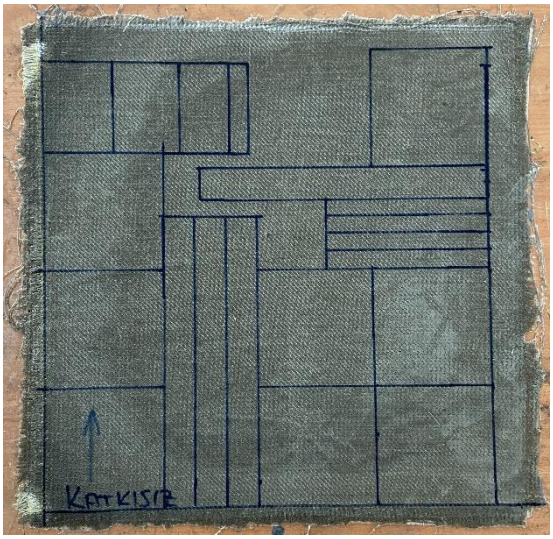


Figure 3.13 Test Sample Cutting Template

Since the cutting allowance of the saw was observed to be 2 mm, the samples were drawn larger than 2 mm in width and length. The wet cutting saw was used to cut the composite panels (Figure 3.14).

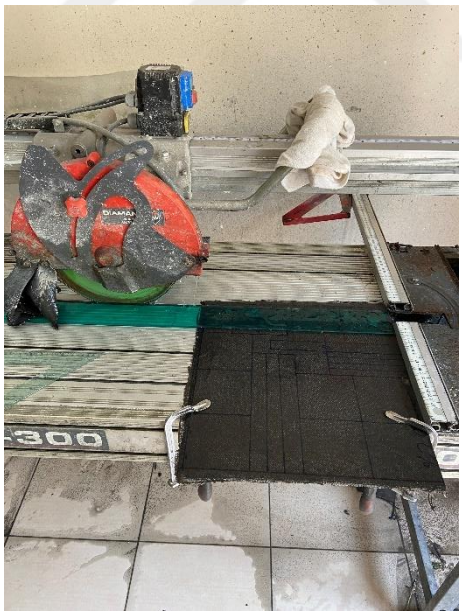


Figure 3.14 Wet Cutting Saw

The samples were sorted separately to avoid mixing and allowed to dry (Figure 3.15).

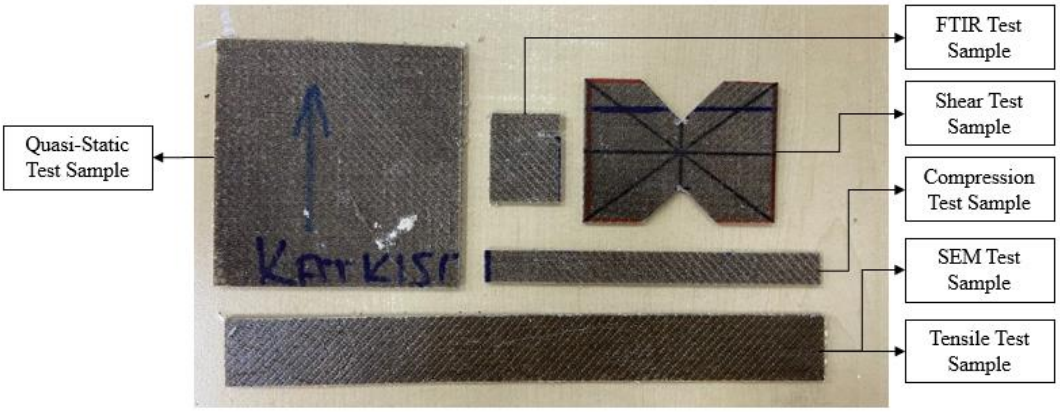


Figure 3.15 Prepared Test Samples

3.2.5 Tensile Test

One of the key mechanical characteristics of materials is their tensile behavior. The tensile test could be used to determine the tensile strength, modulus of elasticity, and Poisson's ratio values of composite materials.

Tensile load is applied to the composites in this research following ASTM-D3039/D3039M-14. Since the composite structure is symmetrical, the tensile test was performed in one direction.

The dimensions of the samples were 25 mm x 250 mm. In order to reduce the tensile test's stress concentration caused by the holding jaws, 25x25 mm plastic tabs were attached to the ends of the tensile samples before they entered the holding jaws (Figure 3.16).



Figure 3.16 Tensile Test Sample

The Shimadzu AG-X 100 kN tensile test equipment at Dokuz Eylül University Department of Mechanical Engineering was used to perform the tensile tests. Appropriate grips for tensile testing are installed on the machine. (Figure 3.17).

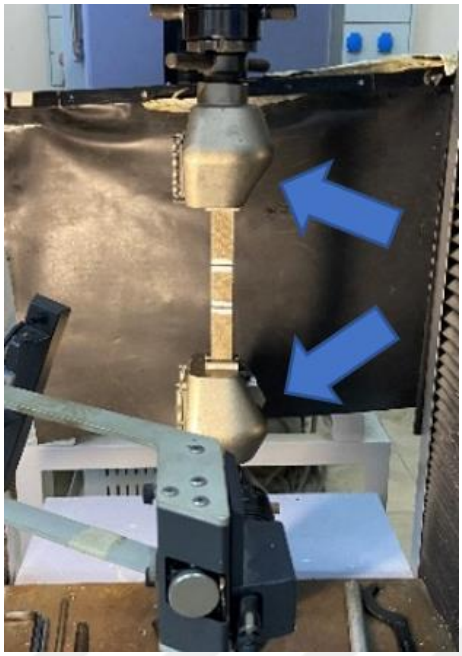


Figure 3.17 Shimadzu AG-X Tensile Test Machine

The machine measured the tensile load, and the strain gage, extensometer, and machine also measured the tensile strains of the samples. In addition, Poisson's ratio and elastic modulus of samples are determined by the strain gauge, which is positioned in both the warp and weft directions. As seen in Figure 3.18, measuring strain values were obtained using the TDS-530 data logger.



Figure 3.18 Tensile Test with Strain Gage

Following the tensile tests, E_1 and υ_{12} are calculated using the following formulas.

$$\sigma_1 = \frac{P_1}{A} \tag{3.1}$$

$$E_1 = E_2 = \frac{\sigma_1}{\varepsilon_1} \tag{3.1}$$

$$\nu_{12} = -\frac{\varepsilon_2}{\varepsilon_1} \tag{3.3}$$

3.2.6 Compression Test

The compressive test was used to determine the material stiffness, strain, and compressive strength. The compression samples were placed in the Shimadzu AG-X test device together with the apparatus and experiments were carried out. The compression apparatus is shown with orange arrow and compression grip apparatus is shown with blue arrows in Figure 3.19. As seen in Figure 3.19, a compression test in accordance with the ASTM-D6641/D6641M-09 standard was performed using a combined loading compression

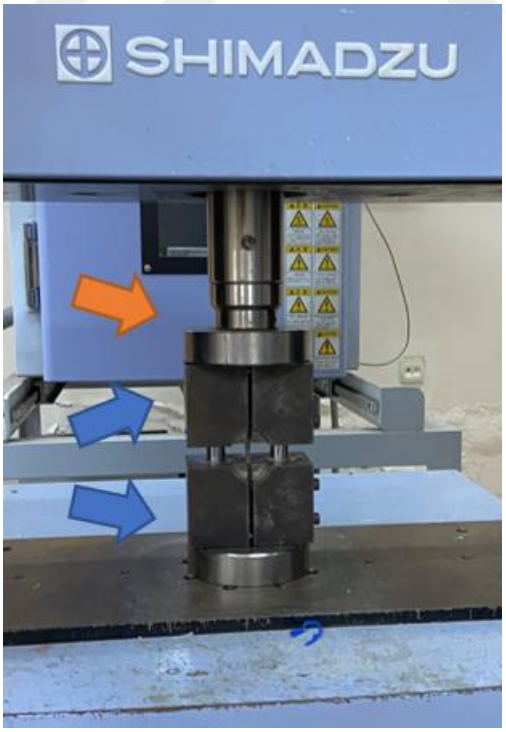


Figure 3.19 Compression Test Device with Apparatus

Shear Test. For the compression test, samples size 13 mm x 140 mm were prepared (Figure 3.20).



Figure 3.20 Compression Test Sample

The compressive strength was determined using equation (3.4).

$$\sigma_C = \frac{P}{A} \tag{3.4}$$

3.2.7 Shear Test

The materials performed the V-Notched Rail shear test in accordance with ASTM-D7078/D7078M-19 standard to determine the shear strength and shear modulus of composites. Figure 3.21 shows the shear test setup. Shear testing was performed using the Shimadzu AG-X 100 kN with shear test equipment. Equipment is shown with blue arrows.

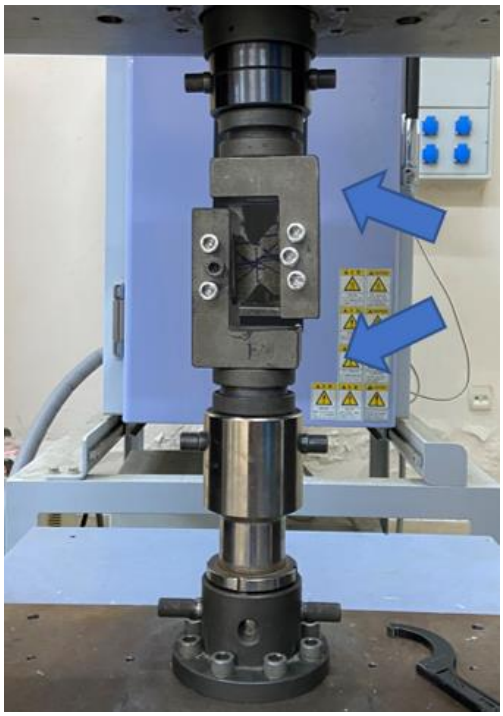


Figure 3.21 Shear Test Setup

Figure 3.22 shows the shear test sample. To determine the shear strain values, the strain gage was positioned at a 45˚ angle on the samples. Equations (3.5) and (3.6) were used to get the shear strength and shear modulus, accordingly.

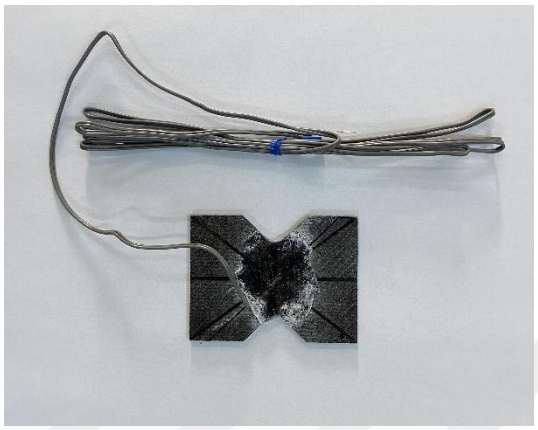


Figure 3.22 Shear Test Sample with Strain Gage

$$\tau_{12} = \frac{P}{A} \tag{3.5}$$

$$G_{12} = \frac{\tau_{12}}{\gamma_{12}} \tag{3.6}$$

3.2.8 Quasi-Static Indentation Test

To determine the material's indentation strength and energy absorption capacity, quasi-static indentation tests were conducted. Drilling forces and drilling tip vertical deformation were used to determine the samples' quasi-static indention behavior of samples. As a result of the test, force deformation curves were drawn. By examining the graphs, the stages of damage initiation, progression and formation of blockage were observed. Deka created a structural model of the force-deformation responses of composites by performing quasi-static experiments. The model is given in Figure 3.23 (Deka, 2008).

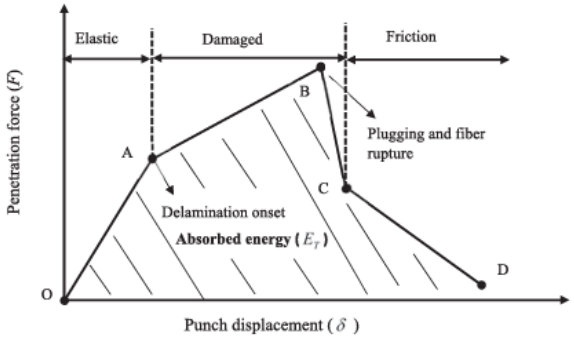


Figure 3.23 Schematics Illustration of a Load-Displacement Curve for Toughened Matrix Composites

The model's examination revealed that the puncture force increased linearly up to the point at which delamination started, when the curves' shape modified. Later, it was observed that the force increased and dropped multiple times before reaching the fiber rupture zone. In earlier research, this condition was described as the tip shattering several strands and entering the obstruction area. The force suddenly decreased following the rupture of the fiber, widening the crack it generated until it reached the friction zone. The experiments were stopped when friction was noticeable at the deformation value. The energy absorbed by materials is expressed by the area under the force-deformation curve. Equation (3.7) below provides the method for computing energy values.

$$E = \int_0^{\delta} F(\delta)\, d\delta \tag{3.7}$$

For quasi-static testing, the Shimadzu AG-X universal testing machine was set up with the proper equipment. The test sample is fixed to the apparatus with 8 bolts to prevent it from slipping. A hemispherical cylinder with diameter of 12.7 mm was used in the tests as shown with blue arrow in Figure 3.24. Quasi-static indention tests were carried out with crosshead speeds of 1.25, 5 and 10 mm/min. according to ASTM D6264 standard.



Figure 3.24 Quasi-Static Indentation Test with Apparatus

Samples with dimensions of 100mmx100mm were prepared for quasi-static indention tests (Figure 3.25).



Figure 3.25 Quasi-Static Indentation Test Sample

3.2.9 SEM Analyses

High-resolution imaging is provided by scanning electron microscopy, or SEM examination, which is helpful for assessing different materials for surface fractures, defects, impurities, or corrosion. To produce a high-resolution image, an electron source, sometimes referred to as an electron gun, blasts a stream of high-energy electrons at a sample. The electron beam is focused by use of electromagnetic lenses.

Upon reaching the sample, the focused stream employs a rectangular raster to examine its surface

When an electron beam interacts with a material, it produces X-rays, backscattered electrons, and secondary electrons. To create an expanded image, these conversations are captured on camera and enlarged (Gleichmann, 2020).

In order to have detailed information about the surface morphological structures of the produced composites, the images obtained using SEM (Scanning Electron Microscope) named ZEISS EVO HD15 (Figure 3.26) were examined in Dokuz Eylül University Science and Technology Application and Research Center.



Figure 3.26 Scanning Electron Microscope ZEISS EVO HD15

The samples that broke as a result of the tensile test were used as SEM test samples. 10mm x 10mm samples were cut from the ruptured area (Figure 3.27).

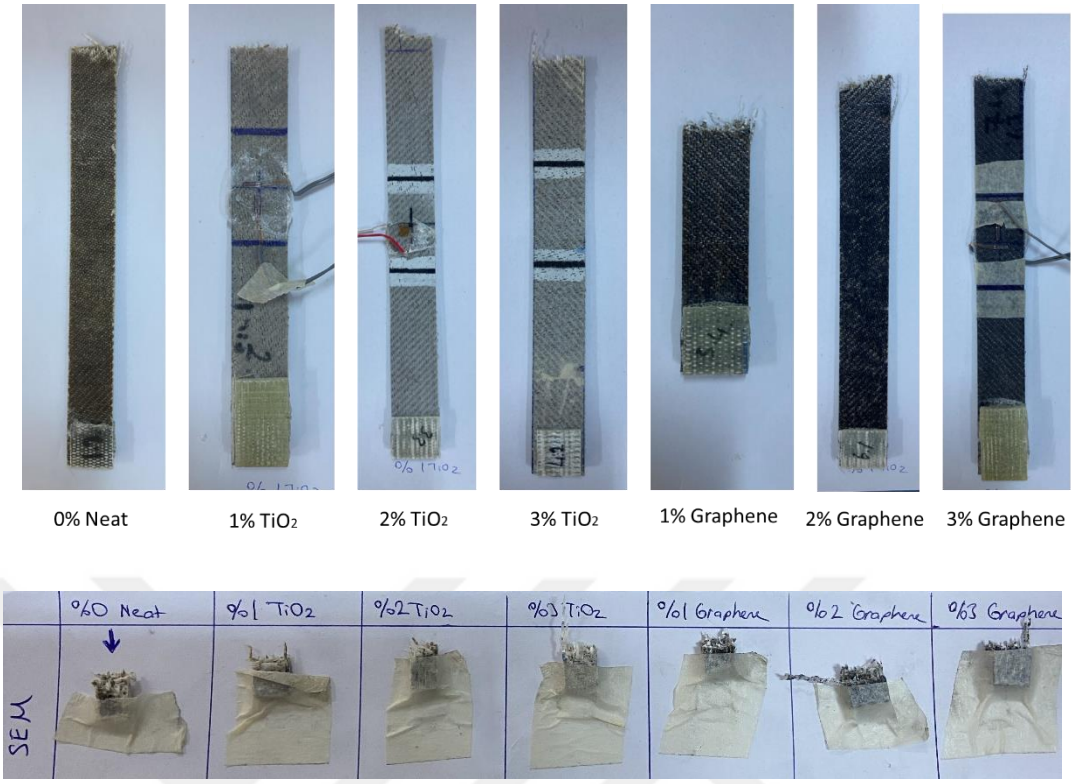


Figure 3.27 SEM Test Samples

Since the test sample is not a conductive material, the samples were coated 30 µm with gold-palladium under vacuum conditions for one hour before SEM analysis (Figure 3.28).

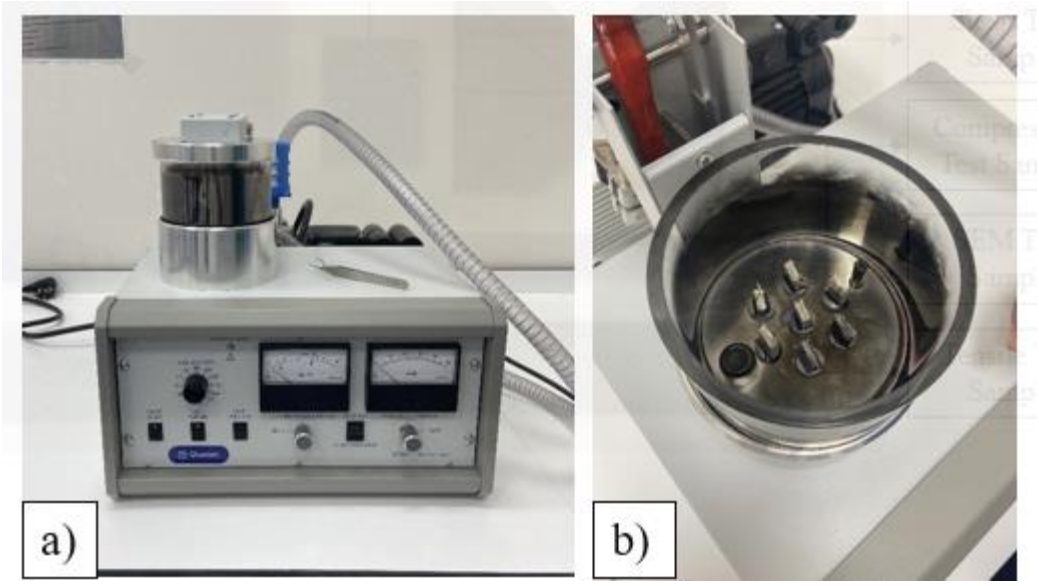


Figure 3.28 a) Coating Device and b) Coated Samples

3.2.10 FTIR Analyses

An analytical method for identifying organic, polymeric, and occasionally inorganic compounds is called FTIR spectroscopy or analysis. Infrared light is used in the FTIR analysis technique to scan test materials and observe chemical characteristics.

When infrared radiation between 10,000 and 100 cm^{-1} is sent through a sample by the FTIR instrument, some of the radiation is absorbed and some is passed over. The sample molecules transform the absorbed radiation into vibrational and/or rotational energy. The final signal at the detector is a spectrum that shows up as the sample's chemical fingerprint and usually ranges from 4000 cm^{-1} to 400 cm^{-1}. The spectrum fingerprints that each molecule or chemical structure produces are unique, which makes Analysis was carried out with the FTIR device Thermo scientific NICOLET iS10 (Figure 3.29) in Dokuz Eylül University Center for Fabrication and Application of Electronic Materials to provide the structure of the bonds in the molecules in the matrix resin.



Figure 3.29 FTIR Device Thermo Scientific NICOLET iS10

FTIR analysis an excellent tool for chemical identification. After samples were cut from the composite plate for other tests, test samples were separated from the remaining plate for FTIR analysis (Figure 3.30).

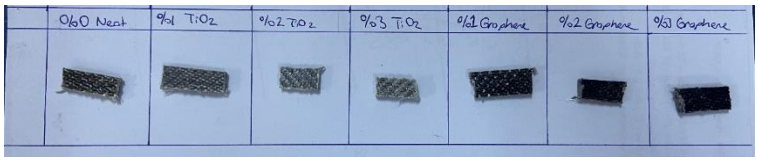


Figure 3.30 FTIR Test Samples

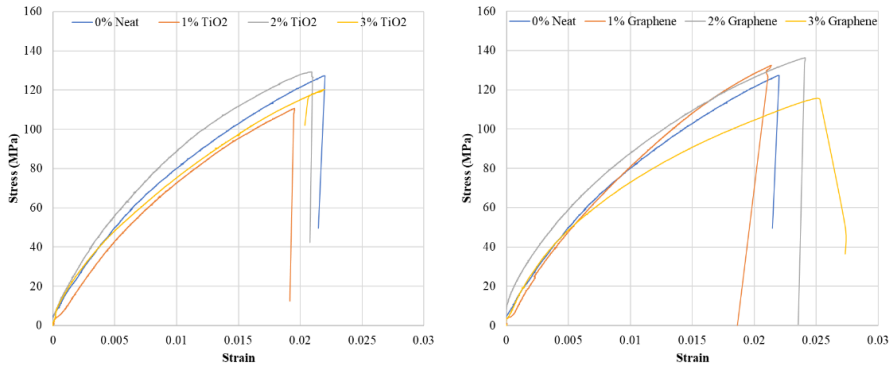
CHAPTER FOUR
EXPERIMENT RESULTS AND DISCUSSION

4.1 Mechanical Test Results

This chapter contains the presentation and analysis of the mechanical test findings for the hybrid woven fabric composites reinforced with different amounts of TiO_2 and few layer graphene. These tests were designed to assess how the tensile, compression, shear and quasi- static indentation properties of the composites were affected by the nanoparticle reinforcement. The hybrid composites were created by adding TiO_2 and graphene nanoparticles in weight percentages of 1-2-3 wt.% to an epoxy resin matrix. Then the matrix was applied to a flax and e-glass hybrid woven fabric. Standardized testing procedures were used to evaluate the mechanical properties, and the findings were carefully examined to identify the ideal concentration of nanoparticles to improve the performance of the composites.

4.1.1 Tensile Test Results

The stress-strain graphs of TiO_2 and few layer graphene reinforced composites obtained from the tensile test are given in Figure 4.1. Upon closer inspection of the graphs, it is evident that the composites' Young modulus changes more noticeably. The young modulus increased in both sample groups with increasing particle reinforcement, by up to 2 wt%.

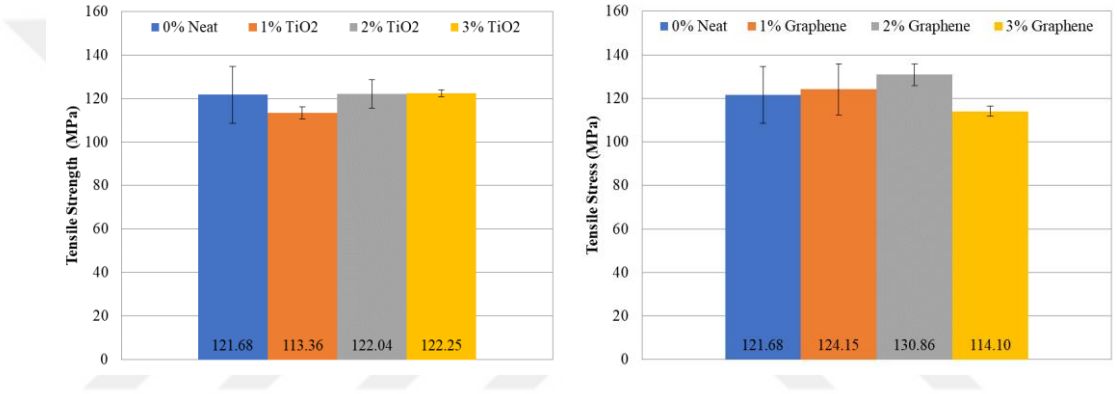


(a) (b)

Figure 4.1 Tensile Stress-Strain Graph of Composites, a) with TiO_2 b) with Few Layer Graphene

Effect of nanoparticle addition on tensile strength is shown in Figure 4.2. It is seen from Figure 4.2-a) that the tensile strength decreases in the composite with 1% TiO_2. Then tensile strength increases by 0.29% for 2% TiO_2 and 0.47% for 3% TiO_2, respectively. Nevertheless, no statistically significant variations were seen between the composites with TiO_2 added and the results of the tensile test.

It is seen form Figure 4.2-b) that the tensile strength increases by 2.03% and 7.54% for the addition of 1% and 2% graphene, respectively. It decreases by 6.24% for 3% graphene addition. It is clear that 2 wt.% graphene added composite has maximum tensile strength.

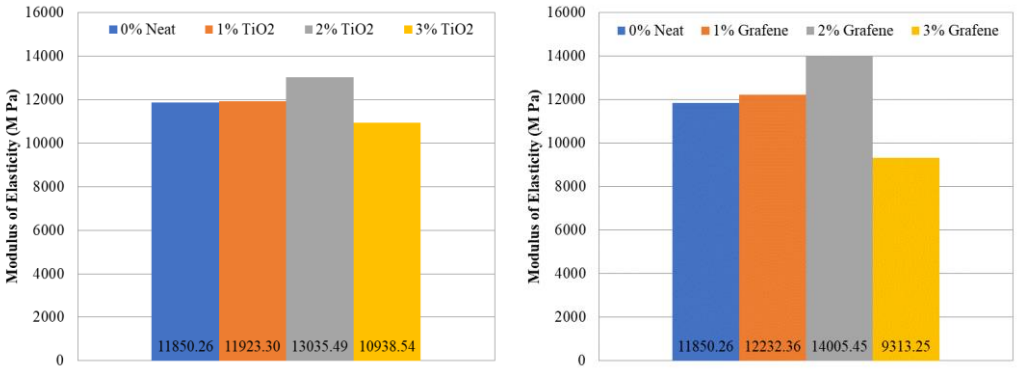


a) b)

Figure 4.2 Tensile Strength Graph of Composites with a) TiO_2, b) Few Layer Graphene

Effect of nanoparticle addition on modulus of elasticity is shown in Figure 4.3. It is seen from Figure 4.3-a) that the modulus of elasticity showed an increase by 0.62% for 1% TiO_2 and maximum value of modulus of elasticity were obtained as 10.00% for composite with 2% TiO_2. The modulus dropped by 7.69% for 3% TiO_2; this could most likely be a result of the accumulation of nanoparticles within the matrix.

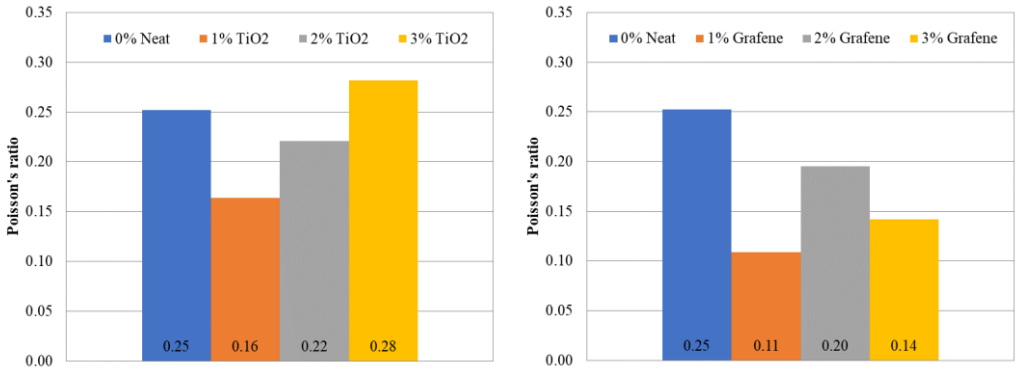
Effect of few layer graphene addition on modulus of elasticity is illustrated in Figure 4.3-b). The modulus of elasticity increases by 3.22% for 1% graphene and by 18.19% for 2% graphene which has the maximum value. However, at 3% graphene, the modulus decreases sharply by 21.41%, likely due to poor dispersion or agglomeration.



a) b)

Figure 4.3 Modulus of elasticity Graph of Composites with a) TiO_2, b) Few Layer Graphene

Using longitudinal and transverse strain gauges, Poisson's ratio was determined. Figure 4.4 illustrates variation of Poisson's ratios according to the additions of TiO_2 and graphene nanoparticles. Addition of 3% TiO_2 increases Poisson's ratio (Figure 4.4-a) while Poisson's ratio decreases for all graphene ratios (Figure 4.6-b).

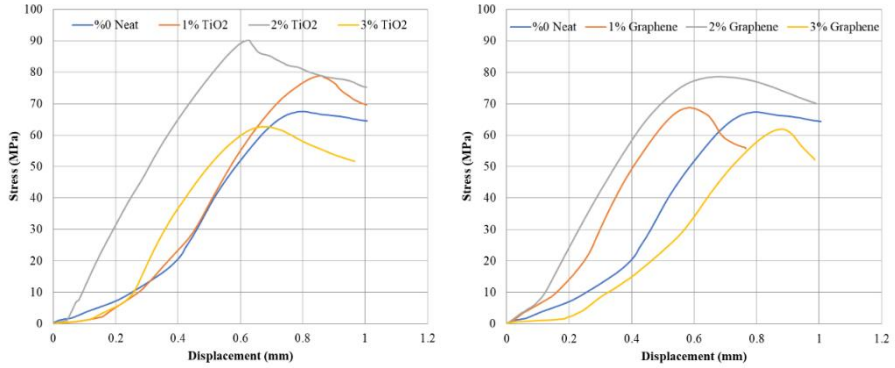


(a) (b)

Figure 4.4 Poisson's Ratio of composites with, a) TiO_2 b) Few Layer Graphene

4.1.2 Compression Test Results

The stress-strain graphs of TiO_2 and few layer graphene reinforced composites obtained from the compression test are given in Figure 4.5. When the graphs were examined, the max compression stress value for both additives increased up to 2% reinforcement.



(a) (b)

Figure 4.5 Compression Stress-Displacement Graph of Composites with, a) TiO_2 , b) Few Layer Graphene

The compression strength shows significant improvement at 1% TiO_2 (by 18.36%) and 2% TiO_2 (by 36.00%), with the highest increase at 2%. However, at 3% TiO_2, the strength drops below the neat sample level, indicating possible negative effects of excessive TiO_2 concentration (by 0.97%). The effect of TiO_2 addition on the compression behavior is also clearly seen statistically (Figure 4.6-a).

The compression strength improves with 1% graphene (by 5.18%) and 2% graphene (by 15.83%), with the highest increase at 2%. At 3% graphene, the strength decreases below the neat sample level (by 5.09%), suggesting a similar trend as observed in tensile tests The effect of graphene addition on the compression behavior is also clearly seen statistically (Figure 4.6-b).

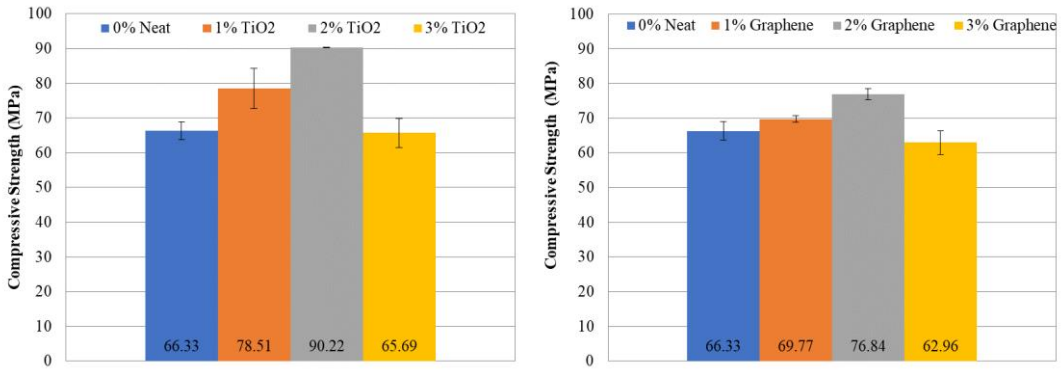
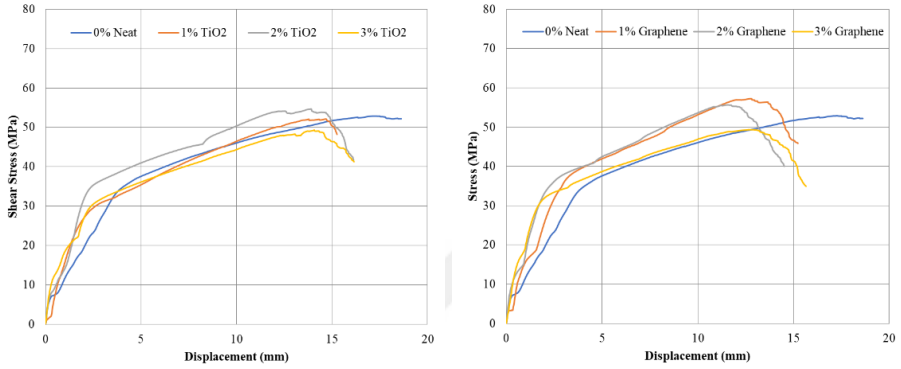


Figure 4.6 Compressive Strength Graph of Composites with a) TiO_2, b) Few Layer Graphene

4.1.3 Shear Test Results

The shear stress-shear strain graphs of TiO_2 and few layer graphene reinforced composites obtained from the shear test are given in Figure 4.10. When the graph was examined, it was observed that the shear strength decreased after 2% for both additives compared to the neat sample.

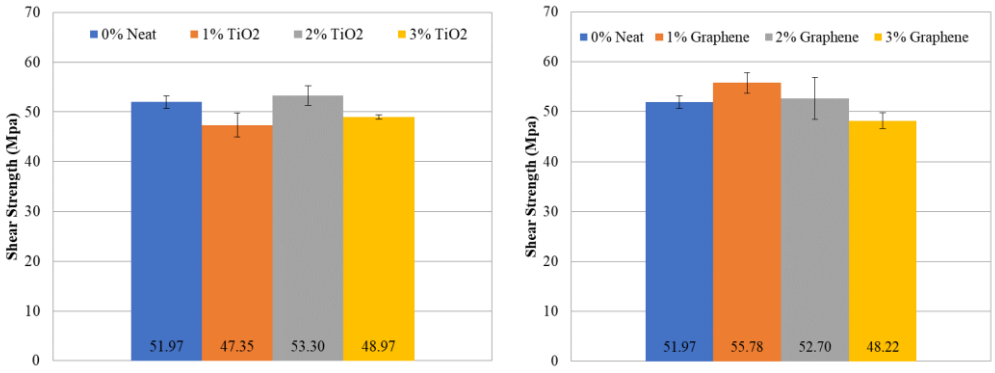


a) b)

Figure 4.7 Shear Stress- Displacement Graph of Composites with a) TiO_2 , b) Few Layer Graphene

Effect of nanoparticle addition on shear strength is shown in Figure 4.8 The shear strength deteriorates with 1 % TiO_2 (by 8.89% %) and improves with 2% TiO_2 (by 2.56%), with the highest increase at 2%. However, at 3%, the strength drops below the neat sample level (by 5.57%), indicating that excessive TiO_2 might weaken shear strength. There were no statistically significant differences found between the shear test findings (Figure 4.8-a).

The shear strength improves with 1% graphene (by 7.34%) but shows a marginal increase at 2% (by 1.41%). At 3% graphene, the shear strength decreases (by 7.21%), indicating that higher concentrations may adversely affect shear performance (Figure 4.8-b).

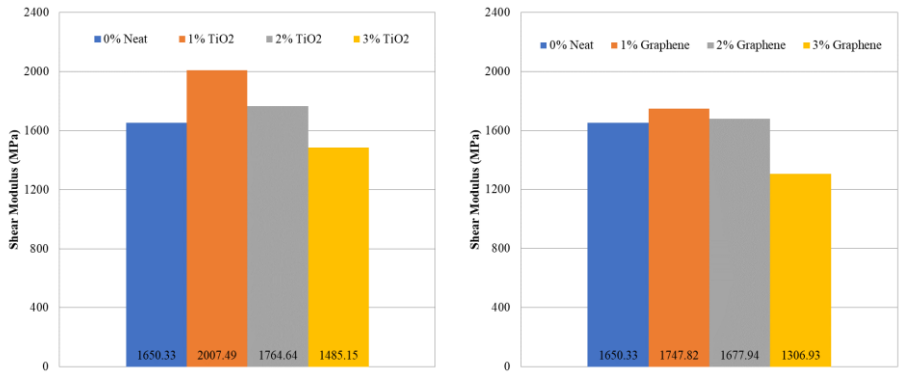


a) b)

Figure 4.8 Shear Strength Graph of Composites with a) TiO_2, b) Few Layer Graphene

Effect of nanoparticle addition on shear modulus is shown in Figure 4.9. The shear modulus increases at 1% TiO_2 (by 21.64%), and 2% TiO_2 (by 6.93%), with the most significant increase at 1%. At 3% TiO_2, the shear modulus decreases (by 10.01%), suggesting that higher concentrations might reduce shear stiffness. (Figure 4.9-a)

The shear modulus shows a slight increase with 1% graphene (by 5.91%) and a marginal increase at 2% graphene (by 1.67%). At 3% graphene, the shear modulus decreases significantly (by 20.81%), indicating potential issues with higher concentrations. (Figure 4.9-b)



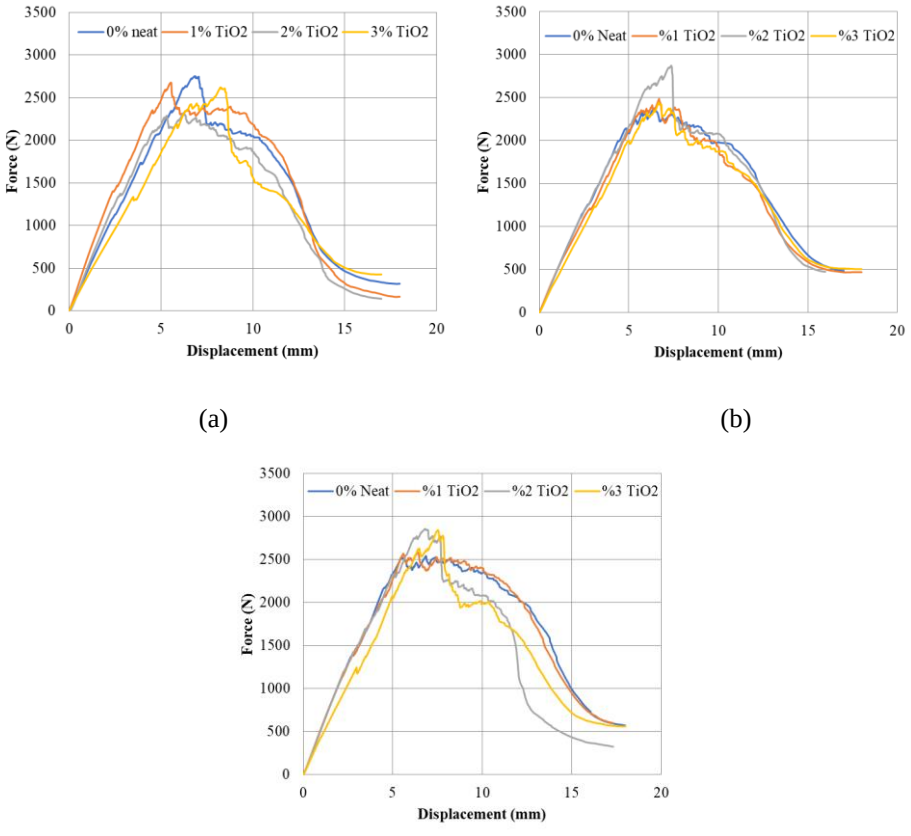
a) b)

Figure 4.9 Shear Modulus Graph of Composites with a) TiO_2, b) Few Layer Graphene

4.1.4 Quasi-Static Indentation Test Results

The performance of TiO_2 and graphene-reinforced composites at varying speeds (1.25 mm/min, 5 mm/min, and 10 mm/min) was assessed by quasi-static indentation testing. The total absorbed energy, the maximum penetration force, and the absorbed energy at the rupture point are the parameters that are examined.

The force - displacement graph of TiO_2 reinforced composites obtained from the quasi-static indentation tests are given in Figure 4.10. Upon closer inspection, these curves revealed that the puncture force increased linearly up until the point at which delamination began, at which time the curves' shape changed. When the force reached the fiber fracture zone, the force repeatedly dropped and increased. The force suddenly decreased after the fiber fracture, widening the crack until it reached the friction zone. The experiments were terminated when it entered the friction zone.



(a) (b)

(c)

Figure 4.10 Force – Displacement Graphs of TiO_2 Added Composites at, a) 1.25 mm/min, b) 5 mm/min, c) 10 mm/ min

The force - displacement graph of graphene reinforced composites obtained from the quasi-static indentation tests are given in Figure 4.11. When the force-displacement graphs are examined, it was observed that graphene entered the friction zone earlier than TiO_2.

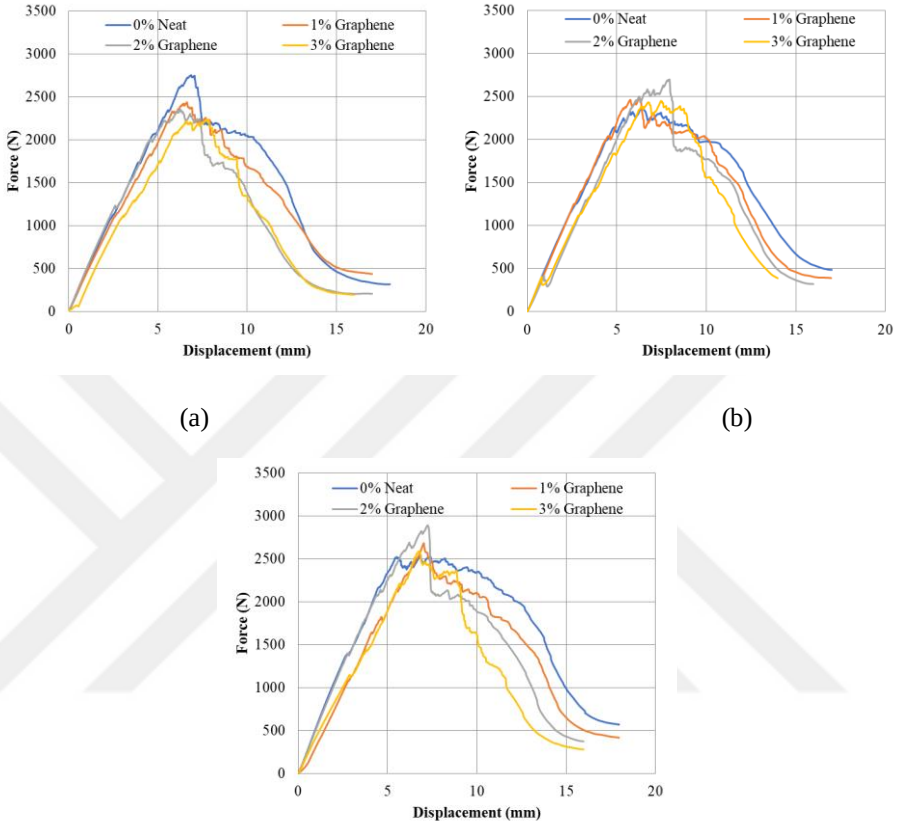


Figure 4.11 Force – Displacement Graphs of Graphene Added Composites at, a) 1.25 mm/min, b) 5 mm/min and c)10 mm/ min

Maximum penetration force results of TiO_2 reinforced composites obtained from the quasi-static indentation tests are given in Table 4.1 and Figure 4.12. At 1.25 mm/min, the maximum penetration force decreases with the addition of TiO_2, at 5 mm/min, 2% TiO2 significantly increases the penetration force, indicating better resistance and at 10 mm/min, 3% TiO_2 shows an increase in penetration force, suggesting enhanced performance at higher strain rates.

Table 4.1 Maximum Penetration Force of TiO_2 Added Composites

	0% Neat (N)	1% TiO_2 (N)	2% TiO_2 (N)	3% TiO_2 (N)
1.25mm / min	2640 ± 104	2599 ± 107	2456 ± 112	2510 ± 182
5 mm / min	2442 ± 149	2496 ± 29	2751 ± 115	2485 ± 58
10 mm / min	2676 ± 125	2594 ± 129	2641 ±288	2829 ± 97

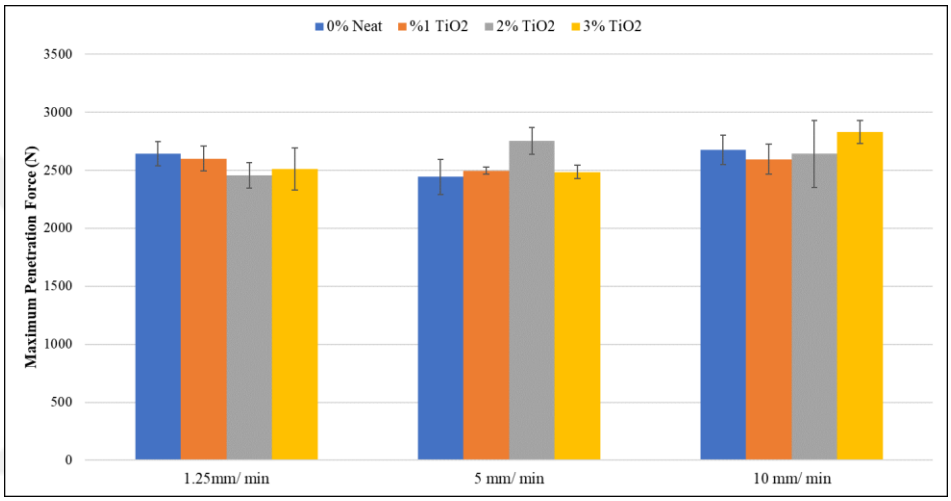


Figure 4.12 Maximum Penetration Forces of TiO_2 Added Composites

Maximum penetration force of graphene reinforced composites obtained from the quasi-static indentation tests are given in Table 4.2 and Figure 4.13. At 1.25 mm/min, the maximum penetration force decreases with the addition of Graphene, at 5 mm/min, 2% Graphene significantly increases the penetration force, indicating better resistance and, at 10 mm/min, 2% Graphene shows a slight increase, but 3% Graphene shows a decrease, suggesting that higher concentrations may not be beneficial at higher strain rates.

Table 4.2 Maximum Penetration Force of Graphene Added Composites

	0% Neat (N)	1% Graphene (N)	2% Graphene (N)	3% Graphene (N)
1.25 mm/min	2640 ± 104	2544 ± 175	2469 ± 160	2280 ± 66
5 mm/min	2442 ± 149	2514 ± 70	2665 ± 216	2470 ± 103
10 mm/min	2676 ± 125	2670 ± 269	2749 ± 180	2599 ± 22

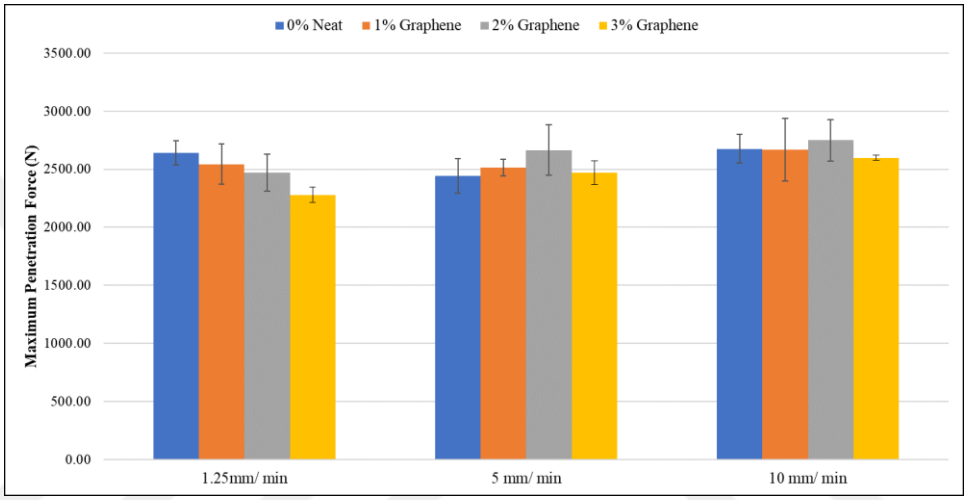
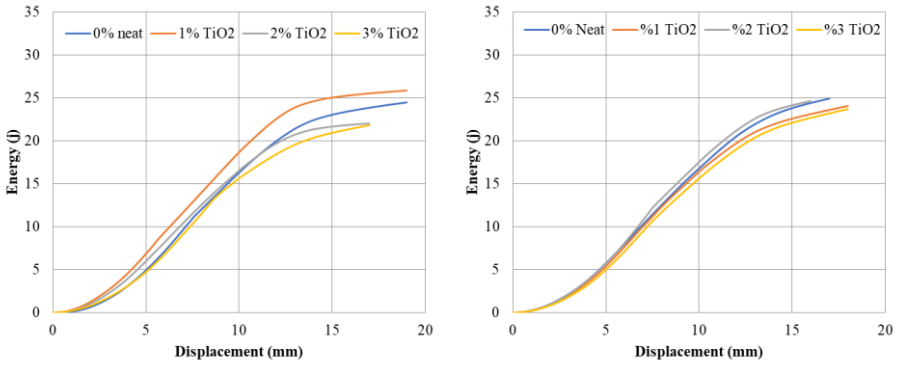
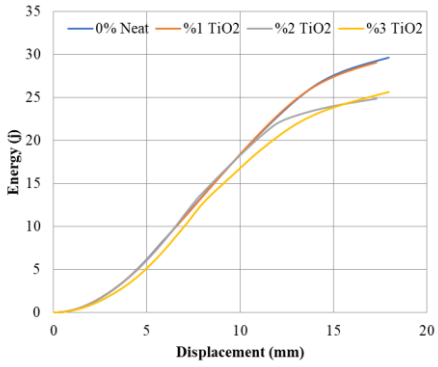


Figure 4.13 Maximum Penetration Forces of Graphene Added Composites

Energy-displacement graphs created using equation 3.7 are given below for TiO_2 addition (Figure 4.14). When the energy-deformation graphs were examined for both nano reinforcements, it was seen that the curves were close to each other until the fiber fracture region, but after this region, differences began to occur between the curves. As the deformation value reached the friction zone, the energy increase rates of all curves decreased.



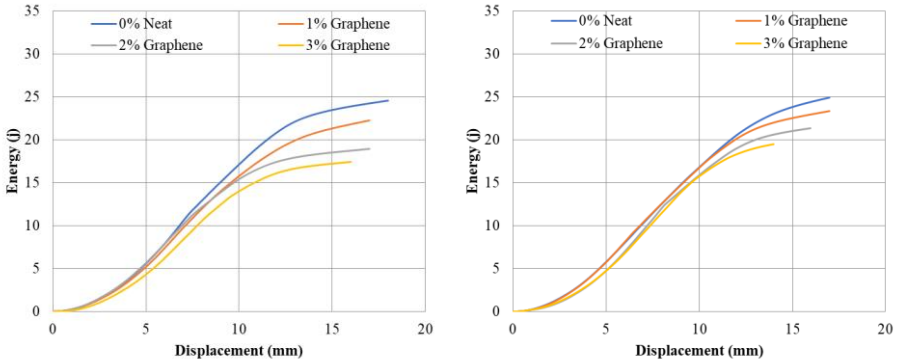
(a) (b)



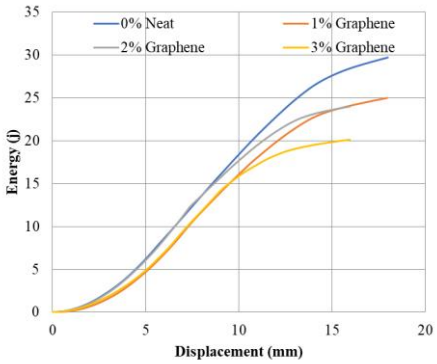
(c)

Figure 4.14 Energy-Displacement Graphs for TiO_2 Added Composites at, a) 1.25 mm/min, b) 5 mm/min and c) 10 mm/ min

Energy-displacement graphs created using equation 3.7 are given below for graphene addition (Figure 4.15).



(a) (b)



(c)

Figure 4.15 Energy-Displacement Graphs for Graphene Added Composites at, a) 1.25 mm/min, b) 5 mm/min and c) 10 mm/ min

The addition of 1% TiO_2 increased the absorbed energy at all test speeds. Absorbed energy of TiO_2 reinforced composites is given in Table 4.3 and Figure 4.16.

Table 4.3 Total Absorbed Energy Graph for TiO_2 Added Composites

	0% Neat (J)	1% TiO_2 (J)	2% TiO_2 (J)	3% TiO_2 (J)
1.25mm/ min	23,82 ± 0,52	26,62 ± 0,91	21,84 ± 1,52	21,55 ± 1,24
5 mm/ min	24,76 ± 0,93	25,28 ± 2,39	25,02 ± 0,41	23,85 ± 0,71
10 mm/ min	28,42 ± 1,81	30,90 ± 1,15	25,31 ± 0,70	25,25 ± 1,26

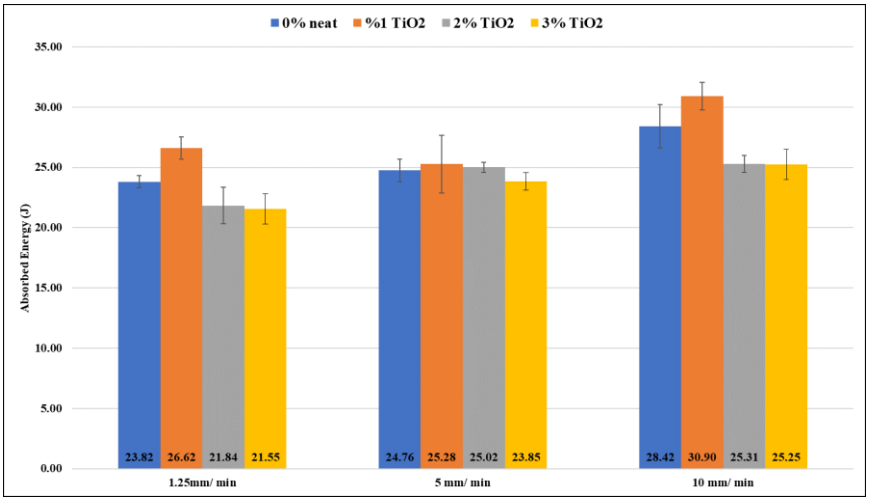


Figure 4.16 Total Absorbed Energy Graph for TiO_2 Added Composites

Absorbed energy of Graphene reinforced composites is given in Table 4.4 and Figure 4.17. Graphene reduced energy absorption capacity of composite at 1-2-3 wt.% nanoparticle addition (Figure 4.17).

Table 4.4 Total Absorbed Energy Graph for Graphene Added Composites

	0% Neat (J)	1% Graphene (J)	2% Graphene (J)	3% Graphene (J)
1.25mm/ min	23,82 ± 0,52	23,03 ± 0,71	20,47 ± 1,33	17,98 ± 1,10
5 mm/ min	24,76 ± 0,93	23,82 ± 1,56	21,80 ± 0,77	19,62 ± 0,49
10 mm/ min	28,42 ± 1,81	25,07 ± 0,65	23,60 ± 0,68	19,71 ± 0,83

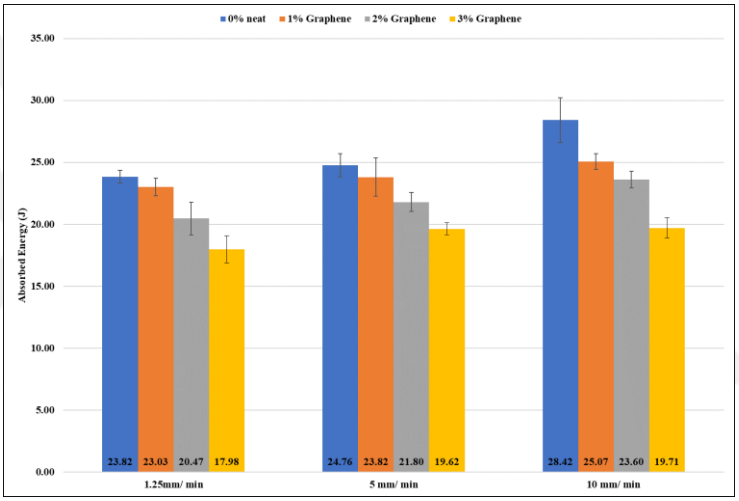


Figure 4.17 Total Absorbed Energy Graph for Graphene Added Composites

4.2 SEM Analysis Results

Images captured with a SEM (Scanning Electron Microscope) (ZEISS EVO HD15) were analyzed to gather comprehensive data regarding the surface morphological structures. SEM analysis was carried out on the fracture surface following the application of the tensile test. The obtained SEM pictures have a zoom size of 500 X and 1K X due to the fringed structure of linen. Neat, TiO_2 added and graphene added composite SEM pictures shown in Figure 4.18, 4.19 and 4.20 respectively.

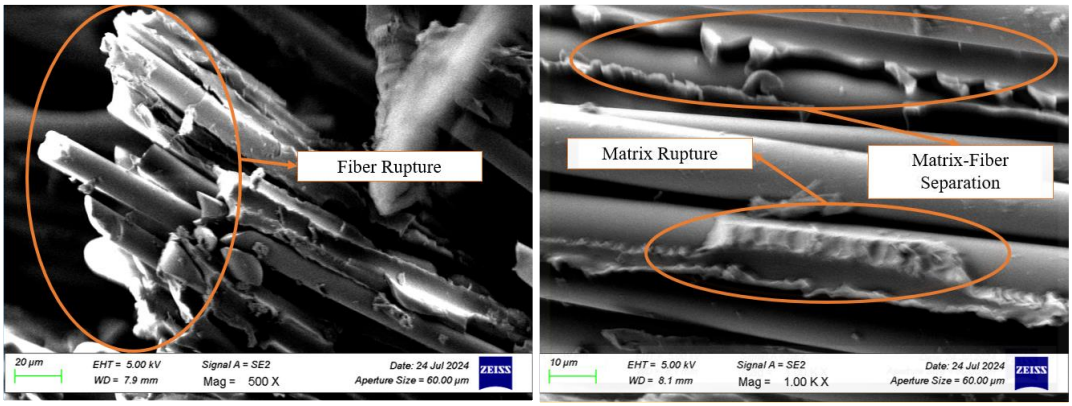


Figure 4.18 SEM Pictures of Neat Composite

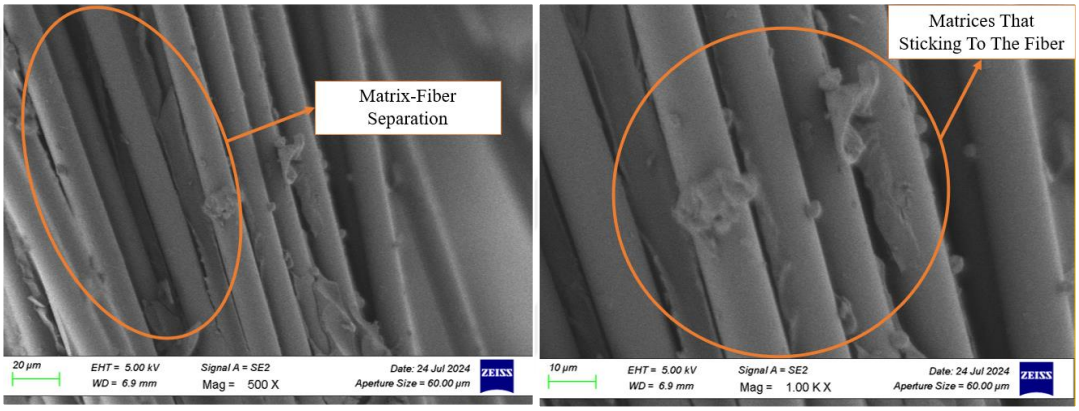


Figure 4.19 SEM Pictures of TiO_2 Added Composite

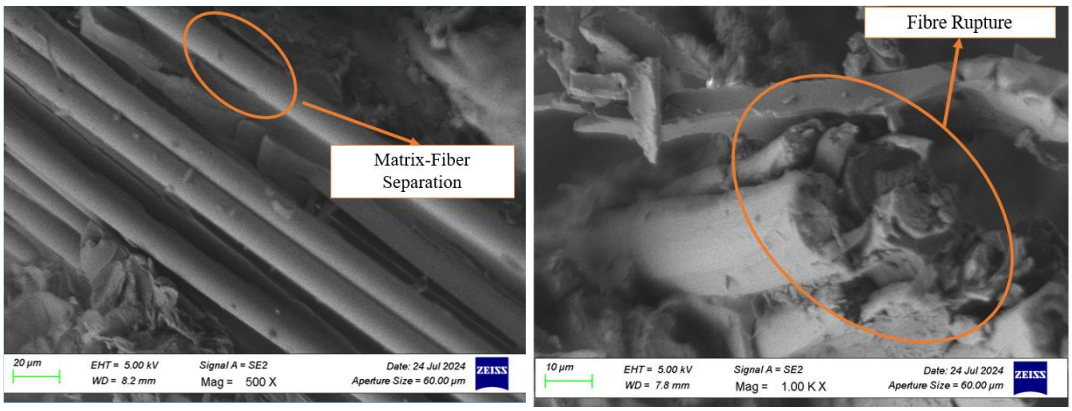


Figure 4.20 SEM Pictures of Graphene Added Composite

4.3 FTIR Analysis Results

FTIR analyzes were carried out to examine the chemical characterizations, functional groups and their effects on the chemical structure of the produced E-glass and flax 2x2 twill hybrid woven fabric reinforced [0˚/90˚/90˚/0˚] layered composites, without nano additives in epoxy resin and with 1-2-3 wt.% nanoparticle additives.

FTIR spectrum analyzes of hybrid woven 0-1-2-3 wt.% TiO_2 added nanocomposites are given in Figure 4.21.

First of all, neat resin samples were investigated. The characteristic wave number range for the stretching vibration of O-H and C-H bonds in polysaccharides is 3660–2900 cm^{-1}. These peaks have been seen in this range. The wide peak seen at 3331 cm^{-1} is indicative of the hydroxyl group's stretching vibration in polysaccharides. As the predominant constituent of plant biomass, cellulose is the most prevalent polysaccharide globally (Rosa, et al., 2010,). Si-O-Si Stretching (peak around 1000-1100 cm^{-1}) suggests the presence of siloxane bonds, indicative of the silicate structure in e-glass fibers, consistent with studies on glass fibers (Grammatikos, Zafari, Evernden, Mottram, & Mitchels, 2015). Together, these peaks indicate the existence of e-glass and flax fibers in the epoxy matrix, emphasizing the contributions of the hybrid composite's natural and synthetic constituents. Additional peaks around this region 500-900 cm^{-1}, corresponding to the Ti-O stretching vibrations, are introduced by the presence of TiO_2 nanoparticles. FTIR measurements on TiO_2 nanoparticles provide evidence for this as the nanoparticle increases, the peak in the graph increases. The appearance of a new peak in this region confirms the presence of TiO_2 nanoparticles, consistent with FTIR studies on TiO_2 (Nkabinde, Moloto, & Matabola, 2020). The inclusion of 1 weight percent TiO_2 nanoparticles may result in reflecting or small absorption changes, which could cause a tiny increase in transmittance, as indicated by the higher transmittance line when compared to the neat composite. Because of the greater interaction and aggregation effects inside the composite, the lower transmittance line suggests that the higher concentration of TiO_2 nanoparticles increases the overall absorption (Huang, Qi, Boey, & Zhang , 2022).

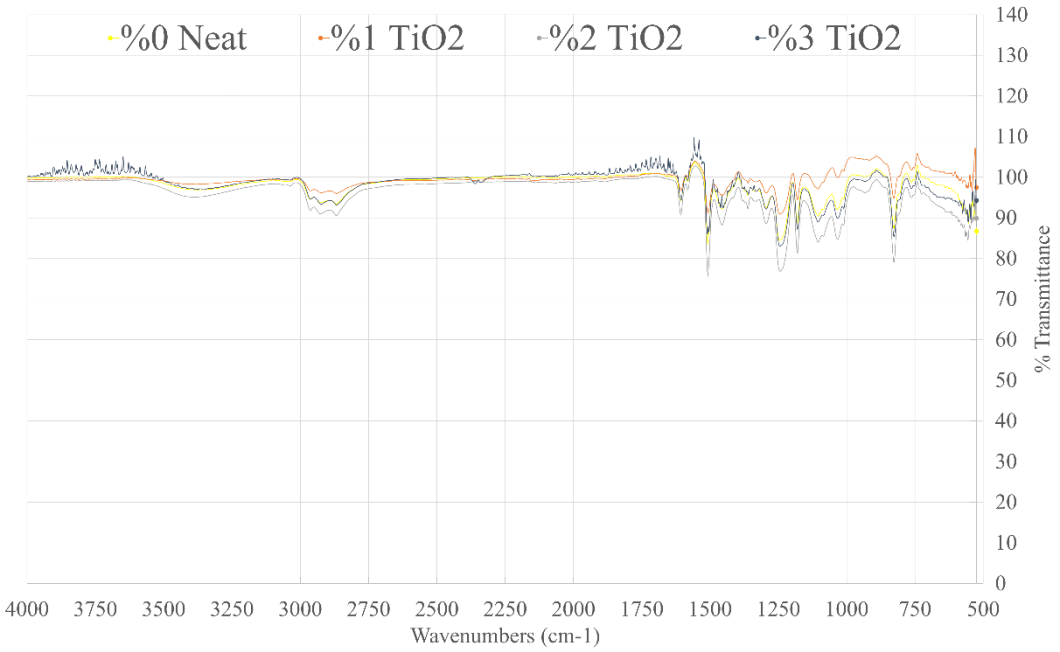


Figure 4.21 FTIR Spectrums of TiO_2 Added Composites

FTIR spectrum analyzes of hybrid woven 0-1-2-3 wt.% graphene added nanocomposites are given in Figure 4.22 The stretching vibrations of C=C bonds, which are the vibrational modes of graphene, are responsible for the peaks in this region (1613 -1580 cm^{-1}), as the amount of graphene in the resin matrix increases, so does its intensity, indicating that the graphene has been successfully incorporated and is interacting with the epoxy structure (Strankowski, Włodarczyk, Piszczyk, & Strank, 2016).

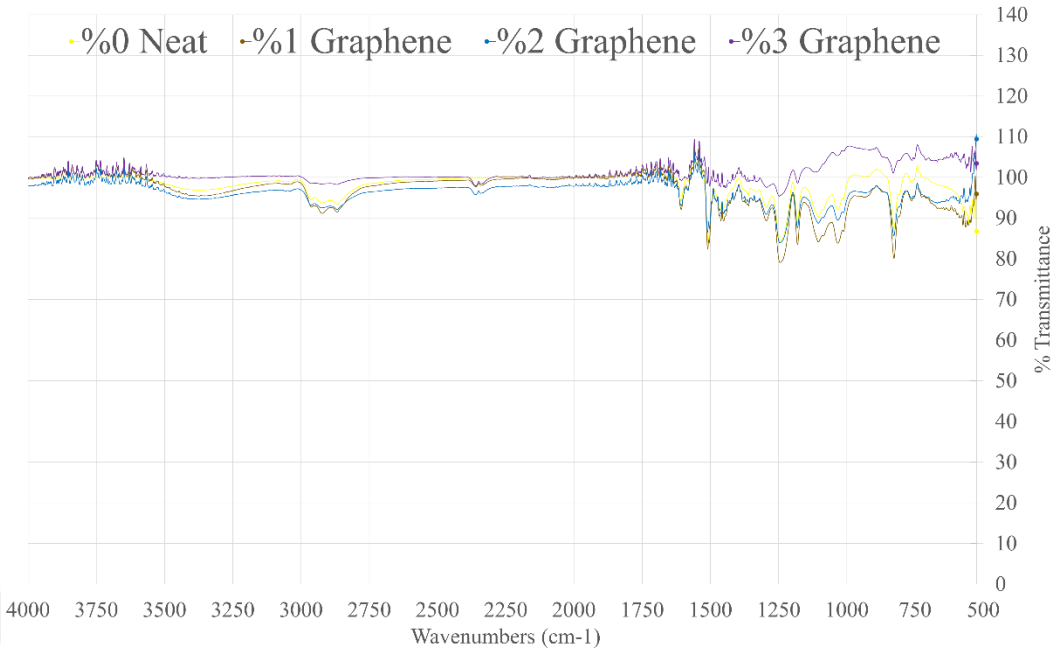


Figure 4.22 FTIR Spectrums of Graphene Added Composites

CHAPTER FIVE
CONCLUSIONS

5.1 Conclusions

In this study, the intraplay glass-flax/epoxy hybrid composites with addition of TiO_2 and few later graphene nanoparticles were manufactured by hand lay-up and vacuum bagging methods. Then tensile, compression and shear properties, and quasi-static indentation behaviors of these composites were investigated, experimentally. SEM and FTIR analyses were also carried out to investigate failure behavior and chemical properties of the composites. From the obtained results, following conclusions can be drawn:

The highest tensile strength increased with 3% TiO_2 by 0.47%. Nevertheless, no statistically significant variations were seen between the composites with TiO_2 added and the results of the tensile test. The modulus of elasticity showed maximum increase with 2% TiO_2 (10.00%). The modulus dropped by 7.69% at 3% TiO_2, most likely as a result of agglomeration of nanoparticles that compromised the integrity of the matrix.

With additions of 3%, the tensile strength of Few Layer Graphene improved 7.54%. Nevertheless, the tensile strength dropped by 6.23% at 3% graphene, indicating that 2 weight percent graphene has superior tensile qualities than 3 wt.% graphene. The modulus of elasticity increased by 18.19% and 3.22% with 1% and 2% of graphene, respectively. The modulus dropped by 21.41% at 3% graphene, most likely as a result of improper dispersion or agglomeration.

The compression test results indicated significant improvements in compression strength with the addition of TiO_2 and Graphene. for TiO_2, the highest increase in compression strength was observed at 2% TiO_2 addition by 36.00%, while at 3%, the strength dropped below the neat sample level by 0.97%. For Graphene, compression strength improved by 5.18% with 1% Graphene and by 15.83% with 2% Graphene. At 3% Graphene, the compression strength decreased below the neat sample level by 5.09%, mirroring the trend observed in tensile tests.

The shear strength showed improvements with the addition of nanoparticles. With the addition of nanoparticles, the shear strength improved. The largest increases for

TiO_2 were noted at 2% by 2.56% but at 3% TiO_2, the strength dropped by 5.77% below the level of the neat sample, indicating that too much TiO_2 could reduce shear strength. Similar trends were observed with Few Layer Graphene, where 1% Graphene improved shear strength by 7.34%, but higher concentrations led to marginal or negative effects. The shear modulus increased significantly with 1% TiO_2 by 21.64% and slightly with 2% TiO_2 by 6.93%. The shear modulus dropped by 10.01% at 3% TiO_2. For Graphene, the shear modulus increased slightly with 1% by 5.91% but decreased significantly at higher concentrations.

The addition of 1% TiO_2 increased the absorbed energy at all test speeds, demonstrating improved energy absorption capacity, according to the quasi-static indentation tests. For Graphene, the energy absorption capacity decreased with increasing nanoparticle concentrations. The maximum penetration force for TiO_2 reinforced composites varied with test speeds, with notable increases observed at certain concentrations and speeds. Similar variations were observed for Graphene, but the overall trend showed a reduction in maximum penetration force with increasing concentrations.

For TiO_2 nanoparticle added composites, the FTIR spectra showed characteristic peaks corresponding to the Ti-O stretching vibrations and this is confirming the incorporation of TiO_2 nanoparticles into the epoxy matrix. For graphene nanoparticle added composites, the FTIR spectra revealed peaks at 1613-1580 cm^{-1} corresponding to the stretching vibrations of C=C bonds, confirming the successful incorporation of graphene into the epoxy matrix. The intensity of these peaks increased with the amount of graphene, indicating enhanced interaction between the graphene and the epoxy structure.

5.2 Recommendations

The outcomes of these experiments reveal insightful information on the mechanical performance of the hybrid composites and a thorough grasp of how nanoparticle reinforcement may be tailored to produce better material qualities. The comprehensive examination of the test outcomes will direct subsequent investigations and real-world implementations in domains where high-performance composite materials are necessary.

Aging behavior and numerical and experimental investigation of the impact behavior of TiO_2 and graphene-added sandwich composites are suggested as topics that can be studied in the future.

REFERENCES

Dhanunjayarao, B., Naidu, N., Phaneendra, Y., & Murty, M. (2022). , Detailed assessment on effect of graphite on mechanical properties of E-Glass/Flax epoxy hybrid polymer composite. *Materials Today: Proceedings*, s. 2214-7853.

Abd El-Baky, M., Attia, M., Abdelhaleem, M., & Hassan, M. (2022). Flax/basalt/E-glass Fibers Reinforced Epoxy. *Journal of Natural Fibers*, s. 954-968.

Balasubramanian, M. (2014). *Composite Materials and Processing.*

Cleveland, B. (2020). *1×1 vs 2×2: Everything You Need to Know About Carbon Fiber Weaves*. vividracing: https://www.vividracing.com/blog/1x1-vs-2x2-everything-you-need-to-know-about-carbon-fiber-weaves/ adresinden alındı

Deka, L. (2008). Multi-site impact response of laminated and sandwich composites. University of Alabama at Birmingham.

Gleichmann, N. (2020). SEM vs TEM.

Grammatikos, S., Zafari, B., Evernden, M., Mottram, J., & Mitchels, J. (2015). Moisture uptake characteristics of a pultruded fibre reinforced polymer flat sheet subjected to hot/wet aging,. *Polymer Degradation and Stability*, s. 407-419.

Hiremath, A., Ambekar, A., Thipperudrappa, S., Rangappa, S., Siengchin, S., & K N , B. (2023). Understanding the interfacial interaction of TiO2 nanoparticles filled glass fiber-epoxy composites through dynamic mechanical analysis. *COMPOSITE INTERFACES*, s. 787–802.

Huang, X., Qi, X., Boey, F., & Zhang , H. (2022). Graphene-based composites. *Chem. Soc. Rev.*, s. 666-686.

Jones, R. (1999). *Mechanics of Composite Materials* . Taylor & Francis.

Kaw, A. (2005). *Mechanics of Composite Materials.*

Krishan, K., & Chawla. (2012). *Composite Materials: Science and Engineering.* Springer.

Mallick, P. (2007). *Fiber-Reinforced Composites: Materials, Manufacturing, and Design.* CRC Press.

Meenakshi, C., & Krishnamoorthy, A. (2018). Preparation and mechanical characterization of flax and glass. *Materials Today: Proceedings*, s. 26934–26940.

Nkabinde, S., Moloto, M., & Matabola, K. (2020). Optimized Loading of TiO2 Nanoparticles into Electrospun Polyacrylonitrile and Cellulose Acetate Polymer Fibers. *Journal of Nanomaterials*.

Prabhu, P., Karthikeyan, B., Ravi Raja Malar Vannan, R., & Balaji, A. (2021). Dynamic mechanical analysis of Silk and Glass (S/G/S)/Pineapple and Glass (P/G/P)/Flax and Glass (F/G/F) reinforced Lannea coromandelica blender hybrid nano composites,. *Journal of Materials Research and Technology,*, s. 2484-2496.

Rosa, M., Medeiros, E., Malmonge, J., Gregorski, K., Wood, D., Mattoso, L., . . . Imam, S. (2010,). Cellulose nanowhiskers from coconut husk fibers: Effect of preparation conditions on their thermal and morphological behavior,. *Carbohydrate Polymers*, pp. 83-92.

Saba, N., Ahir, P., & Jawaid , M. (2014, June 11). A Review on Potentiality of Nano Filler/Natural Fiber Filled Polymer Hybrid Composites. *Polymers*, s. 2247-2273.

Shanmugam, S., & Meenakshisundaram, O. (2023, Aug 12). Experimental investigation of graphene filled flax/E-glass/epoxy hybrid nanocomposites on physical, mechanical, and thermal properties. *Fullerenes, Nanotubes and Carbon Nanostructures*, s. 38-50.

Siengchin, S., & Dangtungee, R. (2014). Polyethylene and polypropylene hybrid composites based on nano silicon dioxide and different flax structures. *Journal of Thermoplastic Composite Materials*, s. 1428–1447.

Strankowski, M., Włodarczyk, D., Piszczyk, Ł., & Strank, J. (2016). Polyurethane Nanocomposites Containing Reduced Graphene Oxide, FTIR, Raman, and XRD Studies. *Journal of Spectroscopy*.

Strong , A. (2006). *Fundamentals of Composites Manufacturing: Materials, Methods and Applications.* Society of Manufacturing Engineers.

Thipperudrappa, S., Hiremath, A., & Nagaraj, B. (2021). Synergistic effect of ZnO and TiO2 nanoparticles on the thermal stability and mechanical properties of glass fiber-reinforced LY556 epoxy composites. *Polymer Composites*, s. 4831-4844.